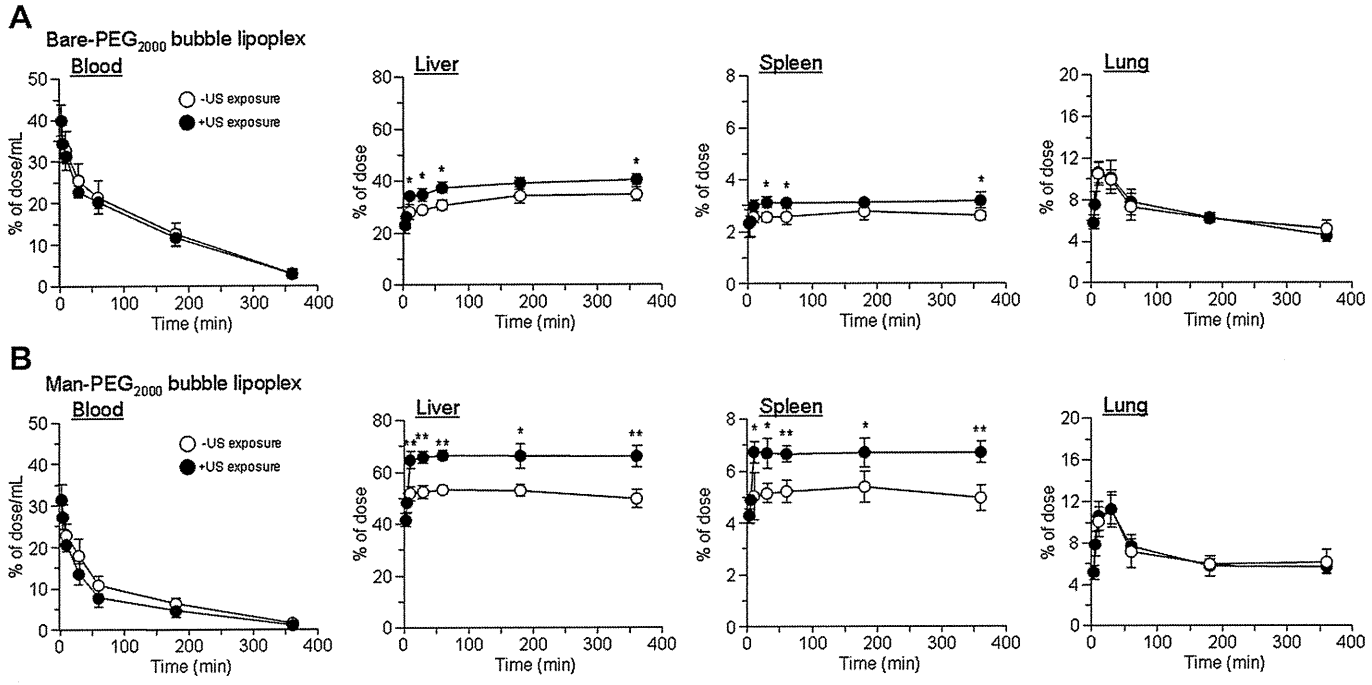

Fig. 7. Tissue distribution of pDNA by Man-PEG_{2000} bubble lipoplexes and US exposure. Tissue distribution after intravenous administration of (A) Bare-PEG_{2000} bubble lipoplexes and (B) Man-PEG_{2000} bubble lipoplexes (50 μg pDNA) with or without US exposure in mice. US was exposed at 5 min after intravenous administration of bubble lipoplexes. Each value represents the mean ± SD ($n = 3$). $^{*}p < 0.05$; $^{**}p < 0.01$, compared with the corresponding group of US exposure.

pCMV-OVA and US exposure significantly enhances the differentiation of helper T cells to Th1 cells, which are pivotal cells for the activation of cytotoxic T lymphocytes (CTL) with high anti-tumor activity, by OVA stimulation.

3.11. Antigen-expressing cell-specific CTL activity in immunized splenic cells

Next, we assessed the CTL activity in the splenic cells harvested from mice immunized by Man-PEG_{2000} bubble lipoplexes and US exposure. Following experiments according to the protocol shown in Fig. 9B, the splenic cells immunized by Man-PEG_{2000} bubble lipoplexes constructed with pCMV-OVA and US exposure showed the highest CTL activity in all groups against E.G7-OVA cells which are the lymphoma cells expressing OVA (Fig. 9D). In contrast, the CTL activity was not observed in EL4 cells which are the lymphoma cells not expressing OVA in all groups (Fig. 9D). These results indicate that the splenic cells immunized by Man-PEG_{2000} bubble lipoplexes constructed with pCMV-OVA and US exposure induce the OVA-expressing cell-specific CTL activity.

3.12. Therapeutic effects against antigen-expressing tumor by DNA vaccination

Finally, we investigated the anti-tumor effects by DNA vaccination using Man-PEG_{2000} bubble lipoplexes and US exposure. Following experiments according to the protocol shown in Fig. 10A, significantly high anti-tumor effects against E.G7-OVA cells were observed in mice immunized by Man-PEG_{2000} bubble lipoplexes constructed with pCMV-OVA and US exposure (Fig. 10B). However, in mice transplanted EL4 cells, no anti-tumor effects were observed in any of the groups (Fig. 10C). Moreover, we investigated the maintenance of DNA vaccine effects following administration of Man-PEG_{2000} bubble lipoplexes and US exposure. According to the protocol shown in Fig. 11A, E.G7-OVA cells were re-transplanted into mice which first-transplanted tumors were completely rejected by DNA vaccination using Man-PEG_{2000} bubble lipoplexes and US exposure. As results, high anti-tumor effects were observed in mice following re-transplantation of E.G7-OVA cells (Fig. 11B); therefore it was demonstrated that DNA vaccine effects obtained by Man-PEG_{2000} bubble lipoplexes constructed with pCMV-OVA and US exposure were maintained for at least 80 days.

4. Discussion

To obtain high therapeutic effects by DNA vaccination using tumor-specific antigen-coding gene, it is essential to transfer the gene selectively and efficiently into the APCs, such as macrophages and dendritic cells [31,32]. However, it is difficult to transfer the gene into the APCs selectively because of the number of APCs is limited in the organ [33]. Since the APCs are expressed a large number of mannose receptors [28,29], we and other groups have developed mannose-modified non-viral carriers for gene delivery to the APCs [7,25,34]. On the other hand, our group also reported that the gene transfection efficiency in the APCs was lower than that in other cells [35]; therefore it is difficult to achieve high gene transfection efficiency to induce high therapeutic effects by DNA vaccination in vivo. In the present study, to establish an APC-selective and efficient gene delivery system, we developed US-responsive and mannose-modified carriers, named Man-PEG_{2000} bubble lipoplexes, which had selectivity to the APCs and responded to US exposure. The gene delivery system using Man-PEG_{2000} bubble lipoplexes and US exposure enabled to achieve markedly high gene expression in macrophages and dendritic cells selectively in vivo, in spite of the handy system used intravenous administration and external US exposure. Moreover, we succeeded in obtaining high anti-tumor effects by applying this method to DNA vaccine therapy using OVA-expressing pDNA.

Firstly, since PEG_{2000}-modification is necessary to enclose US imaging gas stably [12], we prepared Man-PEG_{2000} lipoplexes

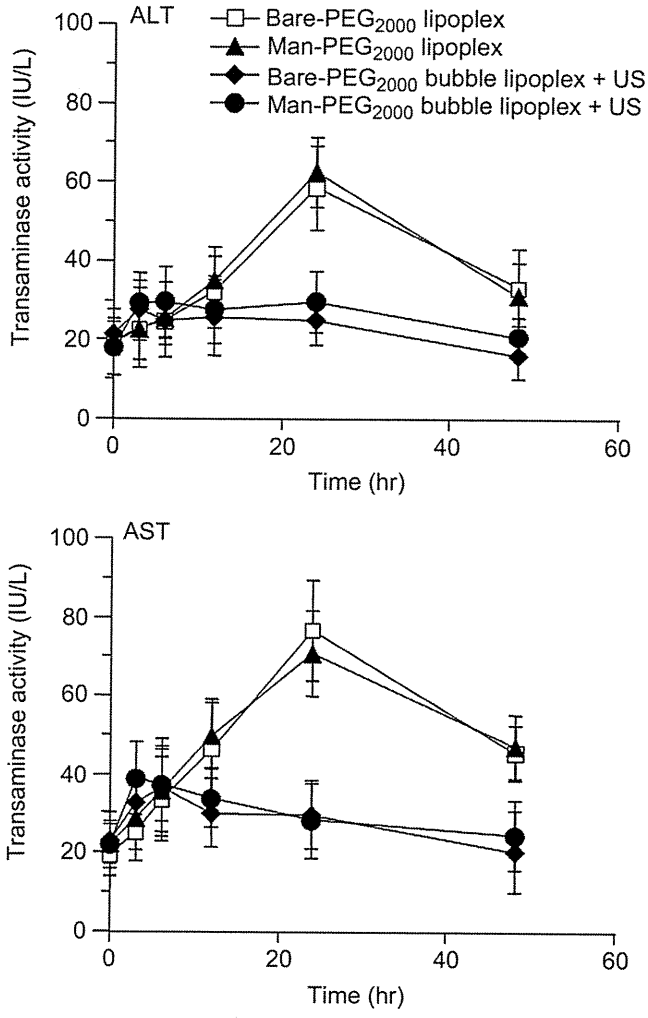

Fig. 8. Liver toxicity by gene transfection using Man-PEG_{2000} bubble lipoplexes and US exposure. Time-course of serum transaminase activities after transfection by Bare-PEG_{2000} lipoplexes, Man-PEG_{2000} lipoplexes, Bare-PEG_{2000} bubble lipoplexes with US exposure and Man-PEG_{2000} bubble lipoplexes with US exposure (50 μg pDNA). Alanine aminotransferase (ALT) and aspartate aminotransferase (AST) in the serum were measured at predetermined times after transfection. Each value represents the mean ± SD ($n = 4$).

containing Man-PEG_{2000} lipids. This Man-PEG_{2000} lipoplexes exhibited mannose receptor-expressing cell-selective gene expression both in vitro and vivo (Fig. 2). On the other hand, the level of gene expression by Man-PEG_{2000} lipoplexes was lower than that by mannosylated lipoplexes without PEG-modification, as reported previously by our group [1,25]. However, this result was considered to be contributed by the reduced interaction with the cell membrane and the reduction of endosomal escape efficiency by PEG_{2000}-modification [36,37]. In the sonoporation method, Tachibana et al. demonstrated that a transient pore is created on the cell membrane followed by the degradation of microbubbles [38]. Then, nucleic acids, such as pDNA, siRNA and oligonucleotides, are introduced into the cell through the generated pore [13,15,16]. Consequently, since the nucleic acids are directly introduced into cytoplasm in the sonoporation method [13,14], it is considered that the low level of transfection efficiency obtained by Man-PEG_{2000} lipoplexes can be overcome by applying sonoporation method. As shown in Figs. 3 and 4, a large amount of pDNA is directly introduced into the cytoplasm and high level of gene expression is observed by gene transfection using Man-PEG_{2000} bubble lipoplexes and US exposure. Therefore, by delivering pDNA to the APCs using Man-PEG_{2000} bubble lipoplexes, it is suggested that high level of gene expression in the APCs can easily achieve by following US exposure in this gene transfection method.

In this study, the level of gene expression obtained by transfection using Man-PEG_{2000} bubble lipoplexes and US exposure was higher than that obtained by Man-PEG_{2000} lipoplexes or Bare-PEG_{2000} bubble lipoplexes with US exposure in the liver and spleen (Fig. 5). Moreover, gene expression by Man-PEG_{2000} bubble lipoplexes and US exposure was observed selectively in the hepatic NPCs and the splenic dendritic cells (Fig. 6), known as mannose receptor-expressing cells [28–30]. Although this selectivity of gene expression was the same as that obtained by mannosylated lipoplexes reported previously by our group [1,25], this level of gene expression was markedly higher. It is considered that this enhanced and cell-selective gene expression is contributed by the increase of interaction with mannose receptor-expressing cells by mannose modification (Supplementary Fig. 1), by the improvement of delivering efficiency of nucleic acids to the targeted organs (Fig. 7) and by the direct introduction of nucleic acids into the cytoplasm of targeted cells followed by US exposure to Man-PEG_{2000} bubble lipoplexes (Figs. 3C and 4B and Supplementary Fig. 4). Moreover, the enhanced gene expression was not observed in the lung, kidney and spleen (Fig. 5G and H). It is guessed that the reason why the enhanced gene expression was not observed in the lung is because US is not spread to the thoracic cavity by the diaphragm, and the reason why the enhanced gene expression was not observed in the kidney and heart was because the distributed amounts of bubble lipoplexes were markedly small. In addition, since the particle size of bubble lipoplexes (approximately 500 nm) is suitable for delivery to the liver and spleen, compared with stabilized liposomes (approximately 100 nm) [39], the gene transfection system using Man-PEG_{2000} bubble lipoplexes and US exposure is a suitable method for the selective delivery of nucleic acids into the mannose receptor-expressing cells in the liver and spleen.

On the other hand, the liver toxicity followed by gene transfection using Man-PEG_{2000} bubble lipoplexes and US exposure was lower than that by Man-PEG_{2000} lipoplexes (Fig. 8). It was reported that the CpG motifs in the pDNA sequence are recognized to Toll-like receptor 9 (TLR9) in the endosomes [40,41]; therefore it has been considered that the production of proinflammatory cytokines, such as TNF-α, IFN-γ and IL-12, could be induced in the lipofection method using liposomes and emulsions, and these cytokines cause liver injury [42]. However, in the gene transfection using Man-PEG_{2000} bubble lipoplexes and US exposure, a large amount of pDNA was directly introduced into the cytoplasm not-mediated endocytosis (Figs. 3C and 4B and Supplementary Fig. 4). Therefore, it is considered that pDNA is not recognized to TLR9 in the endosomes, and consequently liver toxicity followed by transfection using Man-PEG_{2000} bubble lipoplexes and US exposure is low.

In the previous study [16], we developed combination-use method using mannosylated lipoplexes [1] and BLs [12] with US exposure to achieve targeted cell-selective gene transfer. However, this combination-use method is complicated because of the necessity of twice injection of mannosylated lipoplexes and BLs, therefore it is difficult to apply for medical treatments using multiple injection. Moreover, it is considered that the difference of in-vivo distribution characteristics between mannosylated lipoplexes and BLs might be decreased its transfection efficacy. On the other hand, this transfection method using Man-PEG_{2000} bubble lipoplexes and US exposure is handy because of using only once injection of Man-PEG_{2000} bubble lipoplexes and external US exposure. In addition, this method using Man-PEG_{2000} bubble lipoplexes and US exposure overcame the difference of in-vivo distribution of formulations, which might lead to the decrease of

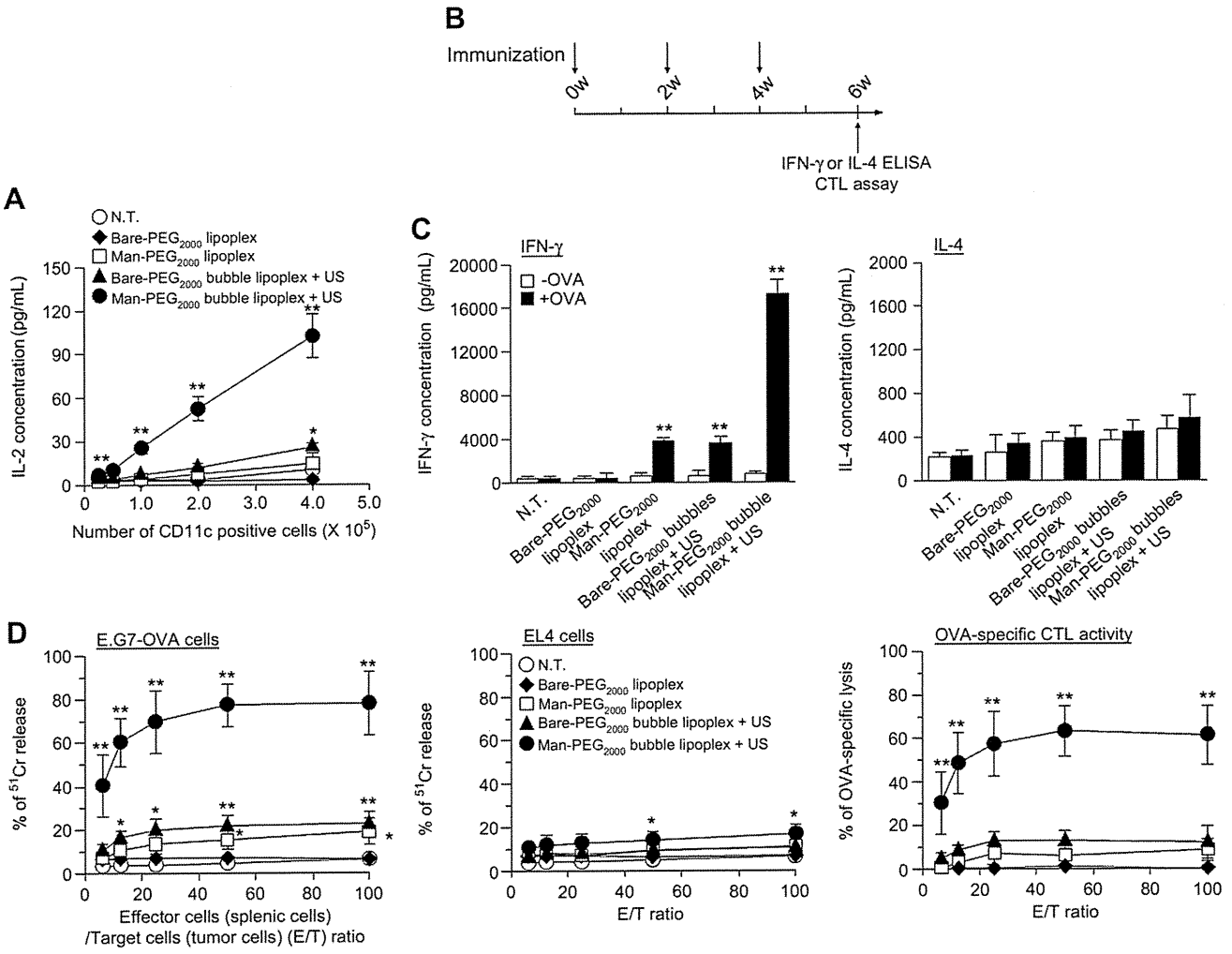

Fig. 9. Cytokine secretion characteristics and CTL activities by DNA vaccination using Man-PEG_{2000} bubble lipoplexes and US exposure. (A) OVA presentation on MHC class I molecules in the splenic $CD11c^+$ cells at 24 h after transfection by Bare-PEG_{2000} lipoplexes, Man-PEG_{2000} lipoplexes, Bare-PEG_{2000} bubble lipoplexes with US exposure and Man-PEG_{2000} bubble lipoplexes with US exposure (50 μg pDNA). OVA presentation on MHC class I molecules was determined by IL-2 level secreted from CD8-OVA1.3 cells co-incubated with the $CD11c^+$ cells isolated from once-immunized mice. Each value represents the mean ± SD ($n = 4$). $^*p < 0.05$; $^{**}p < 0.01$, compared with the corresponding group of N.T. (B) Schedule of immunization for OVA-specific cytokine secretion experiments and CTL assay. (C) OVA-specific IFN-γ and IL-4 secretion from the splenic cells immunized three times biweekly by Bare-PEG_{2000} lipoplexes, Man-PEG_{2000} lipoplexes, Bare-PEG_{2000} bubble lipoplexes with US exposure and Man-PEG_{2000} bubble lipoplexes with US exposure (50 μg pDNA). The splenic cells were collected at 2 weeks after last immunization. After the immunized splenic cells were cultured for 72 h in the absence or presence of 100 μg OVA, IFN-γ and IL-4 secreted in the medium were measured by ELISA. Each value represents the mean + SD ($n = 4$). $^{**}p < 0.01$, compared with the corresponding group of OVA. (D) OVA-specific CTL activities after immunization three times by Bare-PEG_{2000} lipoplexes, Man-PEG_{2000} lipoplexes, Bare-PEG_{2000} bubble lipoplexes with US exposure and Man-PEG_{2000} bubble lipoplexes with US exposure (50 μg pDNA). CTL activities to E.G7-OVA and EL4 cells in the immunized splenic cells were determined by ^{51}Cr release assay. Each value represents the mean ± SD ($n = 4$). $^*p < 0.05$; $^{**}p < 0.01$, compared with the corresponding group of N.T. N.T., non-treatment.

transfection efficiency. In fact, the level of gene expression by this method was higher than that by combination-use method reported previously in the targeted organs (liver and spleen) (Fig. 5) and targeted cells (hepatic NPC and splenic dendritic cells) (Fig. 6); therefore this gene transfection method using Man-PEG_{2000} bubble lipoplexes and US exposure is more suitable for APC-selective gene transfer in vivo.

Since APC-selective and efficient gene expression was observed by transfection using Man-PEG_{2000} bubble lipoplexes and US exposure, effective therapeutic effects are to be expected by applying this transfection method to DNA vaccine therapy, which the targeted cells are the APCs, using tumor-specific antigen-coding pDNA [31,32]. However, since the level of gene expression by transfection using Man-PEG_{2000} bubble lipoplexes and US exposure was reduced sequentially (Supplementary Fig. 6), multiple transfections are essential to obtain more effective vaccine effects against cancer (Supplementary Fig. 7). On the other hand, a 2 week interval was needed to achieve the same level of gene expression by lipoplexes or bubble lipoplexes with US exposure as former transfection in the spleen (Supplementary Fig. 7B and C). Meyer et al. reported that the optimal transfection interval was necessary to achieve high gene expression by the second transfection using lipofection methods because of IFN-γ secretion by intravenous administration of lipoplexes [43]; therefore it is considered that a similar phenomenon is contributed to the sonoporation methods using microbubbles constructed with phospholipids. Based on these findings, we performed the optimization of immunization times (Supplementary Fig. 7) and determined the optimal immunization schedule as shown in Figs. 9B, 10A and 11A.

In DNA vaccine therapy, unlike cancer immunotherapy using tumor-specific antigenic peptides, the peptides expressed as gene products in the cells act as the internal antigen. Since the internal antigens are presented on MHC class I molecules, the strong activation of CTL and high anti-tumor effects are expected in DNA vaccination therapy [44,45]. In this study, by applying this gene transfection method to DNA vaccine therapy using OVA-expressing

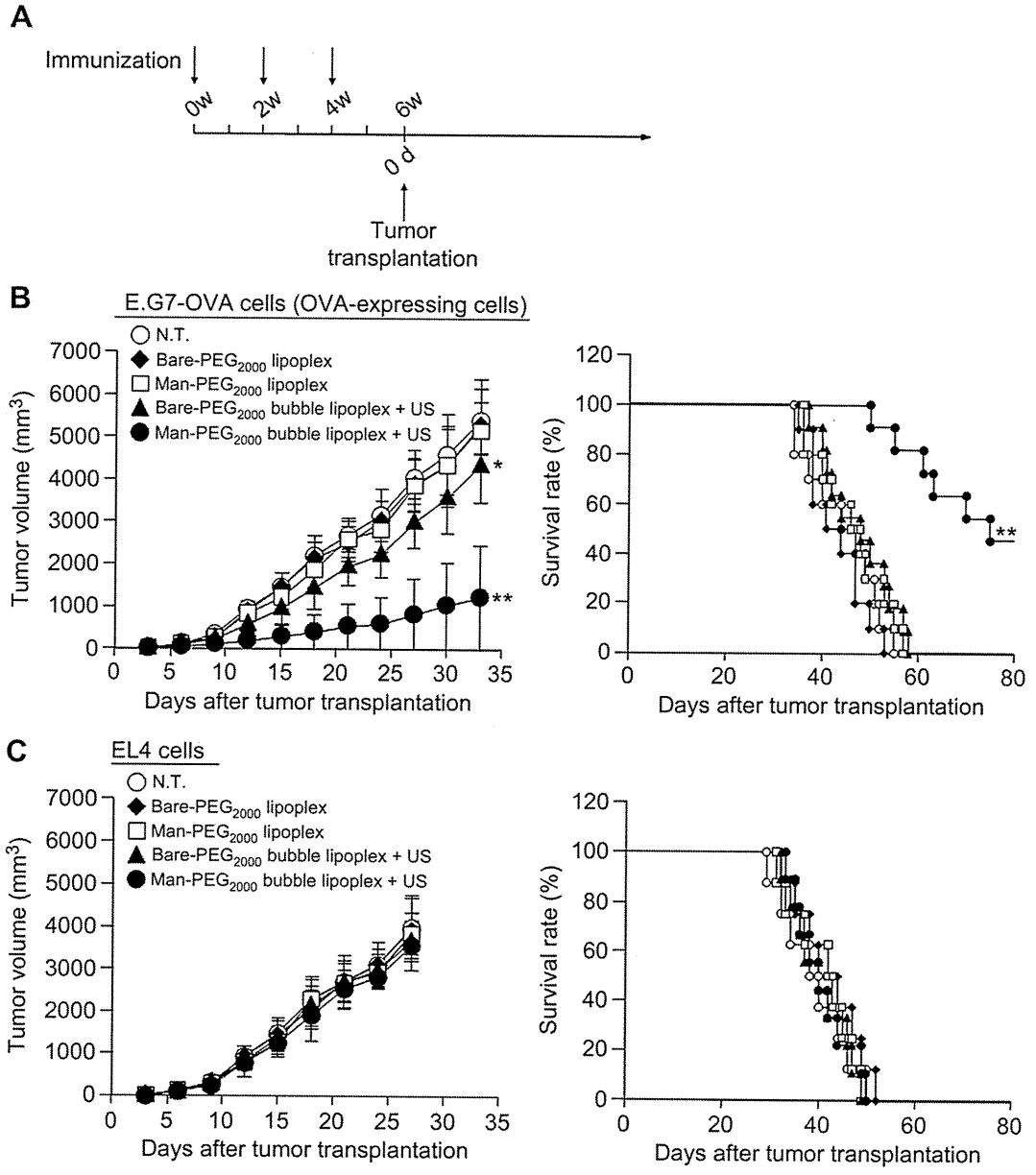

Fig. 10. Anti-tumor effects by DNA vaccination using Man-PEG_{2000} bubble lipoplexes and US exposure. (A) Schedule of immunization for experiments of therapeutic effects. (B, C) Anti-tumor effects by immunization using Bare-PEG_{2000} lipoplexes, Man-PEG_{2000} lipoplexes, Bare-PEG_{2000} bubble lipoplexes with US exposure and Man-PEG_{2000} bubble lipoplexes with US exposure (50 μg pDNA). Two weeks after last immunization, (B) E.G7-OVA cells or (C) EL4 cells (1×10^6 cells) were transplanted subcutaneously into the back of mice ($n = 8–11$). The tumor volume was evaluated (each value represents the mean ± SD) and the survival was monitored up to 80 days after the tumor transplantation. $^*p < 0.05$; $^{**}p < 0.01$, compared with the corresponding group of N.T. N.T., non-treatment.

pDNA, i) the presentation of OVA-peptides on MHC class I molecules of splenic dendritic cells, ii) OVA-specific Th1 cytokine secretion from splenic cells by OVA stimulation and iii) marked activation of CTL against OVA-expressing tumor were observed by gene transfection using Man-PEG_{2000} bubble lipoplexes constructed with pCMV-OVA and US exposure (Fig. 9). Moreover, high and long-term anti-tumor effects against OVA-expressing tumor were observed in mice transfected by Man-PEG_{2000} bubble lipoplexes constructed with pCMV-OVA and US exposure (Figs. 10 and 11). It is considered that these results are contributed by APS-selective and efficient gene transfection efficiency using Man-PEG_{2000} bubble lipoplexes and US exposure. Although more detailed examination by pDNA encoding other tumor-specific antigens, such as gp100 in melanoma or PSA in prostate cancer [45], is necessary, this transfection method by Man-PEG_{2000} bubble lipoplexes and US exposure might be available for DNA vaccine therapy.

The gene transfection method using Man-PEG_{2000} bubble lipoplexes and US exposure was enabled selective and efficient gene transfer to the mannose receptor-expressing cells in the liver such as Kupffer cells and hepatic endothelial cells, which are components of the APCs (Fig. 6A). Therefore, this method is also suitable for anti-inflammatory therapy targeted to Kupffer cells and hepatic endothelial cells, known to play a key role in inflammation [46,47]. In spite of low liver toxicity, since this gene transfection system showed NPC-selective and efficient gene expression in the liver (Fig. 8), better therapeutic effects could be expected by Man-PEG_{2000} bubble lipoplexes constructed with

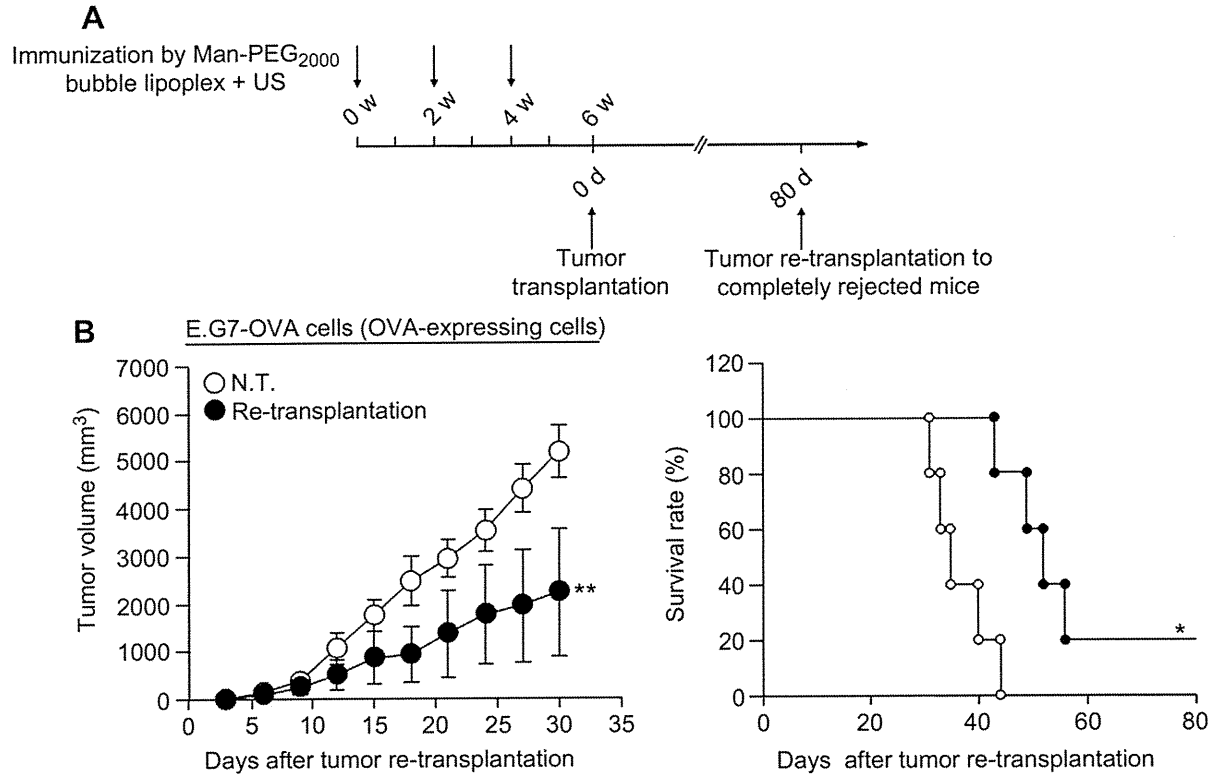

Fig. 11. Maintaining of Anti-tumor effects by DNA vaccination using Man-PEG_{2000} bubble lipoplexes and US exposure. At 80 days after first transplantation of E.G7-OVA cells to immunized mice three times by Man-PEG_{2000} bubble lipoplexes and US exposure, E.G7-OVA cells (1×10^6 cells) were re-transplanted subcutaneously into the back of mice which the first-transplanted tumors were completely rejected ($n = 5$). The tumor volume was evaluated (each value represents the mean ± SD) and the survival was monitored up to 80 days after the tumor re-transplantation. $^*p < 0.05$; $^{**}p < 0.01$, compared with the corresponding group of N.T. N.T., non-treatment.

various types of nucleic acids, such as NF-κB decoy [48], ICAM-1 antisense oligonucleotides [49], with low doses of nucleic acids. Moreover, organ-specific gene expression was observed in US-exposed organ by exposing US to the organ directly after intravenous administration of Man-PEG_{2000} bubble lipoplexes (Supplementary Fig. 5); therefore the beforehand knockdown of inflammatory factors such as NF-κB or ICAM-1 by Man-PEG_{2000} bubble lipoplexes and US exposure might be available for the prevention of ischemia reperfusion injury, a major problem in living donor liver transplantation.

5. Conclusion

In this study, we developed the gene transfection method using Man-PEG_{2000} bubble lipoplexes and US exposure. This transfection method enabled APC-selective and efficient gene expression, and moreover, effective anti-tumor effects was obtained by applying this method to DNA vaccine therapy against cancer. This method could be widely used in a variety of targeted cell-selective and efficient gene transfection methods by substituting mannose with various ligands reported previously [2–6]. In addition, in this gene transfection method, pDNA can directly introduce the nucleic acids into the cells through the transient pores created by US-responsive degradation of bubble lipoplexes, therefore this method could apply to many ligands which are not taken up via endocytosis. These findings make a valuable contribution to overcome the poor introducing efficiency into cytoplasm which is a major obstacle for gene delivery by non-viral vectors, and show that this method is an effective method for in-vivo gene delivery.

Acknowledgements

This work was supported in part by Grant-in-Aid for Scientific Research from the Ministry of Education, Culture, Sports, Science and Technology of Japan, and by Health and Labour Sciences Research Grants for Research on Noninvasive and Minimally Invasive Medical Devices from the Ministry of Health, Labour and Welfare of Japan, and by the Programs for Promotion of Fundamental Studies in Health Sciences of the National Institute of Biomedical Innovation (NIBIO), and by the Japan Society for the Promotion of Sciences (JSPS) through a JSPS Research Fellowship for Young Scientists.

Appendix. Supplementary data

Supplementary data associated with this article can be found, in the online version, at doi:10.1016/j.biomaterials.2010.06.058.

References

[1] Kawakami S, Sato A, Nishikawa M, Yamashita F, Hashida M. Mannose receptor-mediated gene transfer into macrophages using novel mannosylated cationic liposomes. Gene Ther 2000;7:292–9.
[2] Schiffelers RM, Koning GA, ten Hagen TL, Fens MH, Schraa AJ, Janssen AP, et al. Anti-tumor efficacy of tumor vasculature-targeted liposomal doxorubicin. J Control Release 2003;91:115–22.
[3] Torchilin VP, Levchenko TS, Rammohan R, Volodina N, Papahadjopoulos-Sternberg B, D'Souza GG. Cell transfection in vitro and in vivo with nontoxic TAT peptide–liposome–DNA complexes. Proc Natl Acad Sci U S A 2003;100:1972–7.
[4] Kirpotin DB, Drummond DC, Shao Y, Shalaby MR, Hong K, Nielsen UB, et al. Antibody targeting of long-circulating lipidic nanoparticles does not increase tumor localization but does increase internalization in animal models. Cancer Res 2006;66:6732–40.

[5] Goldstein D, Gofrit O, Nyska A, Benita S. Anti-HER2 cationic immunoemulsion as a potential targeted drug delivery system for the treatment of prostate cancer. Cancer Res 2007;67:269–75.
[6] Oba M, Aoyagi K, Miyata K, Matsumoto Y, Itaka K, Nishiyama N, et al. Polyplex micelles with cyclic RGD peptide ligands and disulfide cross-links directing to the enhanced transfection via controlled intracellular trafficking. Mol Pharmacol 2008;5:1080–92.
[7] Sheng KC, Kalkanidis M, Pouniotis DS, Esparon S, Tang CK, Apostolopoulos V, et al. Delivery of antigen using a novel mannosylated dendrimer potentiates immunogenicity in vitro and in vivo. Eur J Immunol 2008;38:424–36.
[8] Satkauskas S, Bureau MF, Puc M, Mahfoudi A, Scherman D, Miklavcic D, et al. Mechanisms of in vivo DNA electrotransfer: respective contributions of cell electropermeabilization and DNA electrophoresis. Mol Ther 2002;5: 133–40.
[9] Mukai H, Kawakami S, Kamiya Y, Ma F, Takahashi H, Satake K, et al. Pressure-mediated transfection of murine spleen and liver. Hum Gene Ther 2009;20:1157–67.
[10] Nishikawa M, Nakayama A, Takahashi Y, Fukuhara Y, Takakura Y. Reactivation of silenced transgene expression in mouse liver by rapid, large-volume injection of isotonic solution. Hum Gene Ther 2008;19:1009–20.
[11] Hernot S, Klibanov AL. Microbubbles in ultrasound-triggered drug and gene delivery. Adv Drug Deliv Rev 2008;60:1153–66.
[12] Suzuki R, Takizawa T, Negishi Y, Utoguchi N, Sawamura K, Tanaka K, et al. Tumor specific ultrasound enhanced gene transfer in vivo with novel liposomal bubbles. J Control Release 2008;125:137–44.
[13] Negishi Y, Endo Y, Fukuyama T, Suzuki R, Takizawa T, Omata D, et al. Delivery of siRNA into the cytoplasm by liposomal bubbles and ultrasound. J Control Release 2008;132:124–30.
[14] Lentacker I, Geers B, Demeester J, De Smedt SC, Sanders NN. Design and evaluation of doxorubicin-containing microbubbles for ultrasound-triggered doxorubicin delivery: cytotoxicity and mechanisms involved. Mol Ther 2010; 18:101–8.
[15] Liu Y, Miyoshi H, Nakamura M. Encapsulated ultrasound microbubbles: therapeutic application in drug/gene delivery. J Control Release 2006;114:89–99.
[16] Un K, Kawakami S, Suzuki R, Maruyama K, Yamashita F, Hashida M. Enhanced transfection efficiency into macrophages and dendritic cells by the combination method using mannosylated lipoplexes and bubble liposomes with ultrasound exposure. Hum Gene Ther 2010;21:65–74.
[17] Kawabata K, Takakura Y, Hashida M. The fate of plasmid DNA after intravenous injection in mice: involvement of scavenger receptors in its hepatic uptake. Pharm Res 1995;12:825–30.
[18] Potter NS, Harding CV. Neutrophils process exogenous bacteria via an alternate class I MHC processing pathway for presentation of peptides to T lymphocytes. J Immunol 2001;167:2538–46.
[19] Hattori Y, Suzuki S, Kawakami S, Yamashita F, Hashida M. The role of dioleoylphosphatidylethanolamine (DOPE) in targeted gene delivery with mannosylated cationic liposomes via intravenous route. J Control Release 2005;108:484–95.
[20] Hattori Y, Kawakami S, Lu Y, Nakamura K, Yamashita F, Hashida M. Enhanced DNA vaccine potency by mannosylated lipoplex after intraperitoneal administration. J Gene Med 2006;8:824–34.
[21] Lee YC. 2-Imino-2-methoxyethyl 1-thioglycosides: new reagents for attaching sugars to proteins. Biochemistry 1976;15:3956–63.
[22] Wang LH, Rothberg KG, Anderson RG. Mis-assembly of clathrin lattices on endosomes reveals a regulatory switch for coated pit formation. J Cell Biol 1993;123:1107–17.
[23] Akiyama T, Ishida J, Nakagawa S, Ogawara H, Watanabe S, Itoh N, et al. Genistein, a specific inhibitor of tyrosine-specific protein kinases. J Biol Chem 1987;262:5592–5.
[24] West MA, Bretscher MS, Watts C. Distinct endocytotic pathways in epidermal growth factor-stimulated human carcinoma A431 cells. J Cell Biol 1989;109:2731–9.
[25] Hattori Y, Kawakami S, Nakamura K, Yamashita F, Hashida M. Efficient gene transfer into macrophages and dendritic cells by in vivo gene delivery with mannosylated lipoplex via the intraperitoneal route. J Pharmacol Exp Ther 2006;318:828–34.
[26] Rigby PWJ, Dieckmann M, Rhodes C, Berg P. Labeling deoxyribonucleic acid to high specific activity in vitro by nick translation with DNA polymerase I. J Mol Biol 1977;113:237–51.
[27] Kawakami S, Wong J, Sato A, Hattori Y, Yamashita F, Hashida M. Biodistribution characteristics of mannosylated, fucosylated, and galactosylated liposomes in mice. Biochim Biophys Acta 2000;1524:258–65.
[28] Taylor PR, Gordon S, Martinez-Pomares L. The mannose receptor: linking homeostasis and immunity through sugar recognition. Trends Immunol 2005;26:104–10.
[29] Tacken PJ, de Vries IJ, Torensma R, Figdor CG. Dendritic-cell immunotherapy: from ex vivo loading to in vivo targeting. Nat Rev Immunol 2007;7:790–802.
[30] Kurts C. CD11c: not merely a murine DC marker, but also a useful vaccination target. Eur J Immunol 2008;38:2072–5.
[31] Steinman RM, Banchereau J. Taking dendritic cells into medicine. Nature 2007;449:419–26.
[32] Hume DA. Macrophages as APC and the dendritic cell myth. J Immunol 2008;181:5829–35.
[33] Liu K, Waskow C, Liu X, Yao K, Hoh J, Nussenzweig M. Origin of dendritic cells in peripheral lymphoid organs of mice. Nat Immunol 2007;8:578–83.
[34] Abe Y, Kuroda Y, Kuboki N, Matsushita M, Yokoyama N, Kojima N. Contribution of complement component C3 and complement receptor type 3 to carbohydrate-dependent uptake of oligomannose-coated liposomes by peritoneal macrophages. J Biochem 2008;144:563–70.
[35] Sakurai F, Inoue R, Nishino Y, Okuda A, Matsumoto O, Taga T, et al. Effect of DNA/liposome mixing ratio on the physicochemical characteristics, cellular uptake and intracellular trafficking of plasmid DNA/cationic liposome complexes and subsequent gene expression. J Control Release 2000;66:255–69.
[36] Song LY, Ahkong QF, Rong Q, Wang Z, Ansell S, Hope MJ, et al. Characterization of the inhibitory effect of PEG-lipid conjugates on the intracellular delivery of plasmid and antisense DNA mediated by cationic lipid liposomes. Biochim Biophys Acta 2002;1558:1–13.
[37] Deshpande MC, Davies MC, Garnett MC, Williams PM, Armitage D, Bailey L, et al. The effect of poly(ethylene glycol) molecular architecture on cellular interaction and uptake of DNA complexes. J Control Release 2004;97:143–56.
[38] Tachibana K, Uchida T, Ogawa K, Yamashita N, Tamura K. Induction of cell-membrane porosity by ultrasound. Lancet 1999;353:1409.
[39] Ishida O, Maruyama K, Sasaki K, Iwatsuru M. Size-dependent extravasation and interstitial localization of polyethyleneglycol liposomes in solid tumor-bearing mice. Int J Pharm 1999;190:49–56.
[40] Latz E, Schoenemeyer A, Visintin A, Fitzgerald KA, Monks BG, Knetter CF, et al. TLR9 signals after translocating from the ER to CpG DNA in the lysosome. Nat Immunol 2004;5:190–8.
[41] Leifer CA, Brooks JC, Hoelzer K, Lopez J, Kennedy MN, Mazzoni A, et al. Cytoplasmic targeting motifs control localization of toll-like receptor 9. J Biol Chem 2006;281:35585–92.
[42] Tousignant JD, Gates AL, Ingram LA, Johnson CL, Nietupski JB, Cheng SH, et al. Comprehensive analysis of the acute toxicities induced by systemic administration of cationic lipid: plasmid DNA complexes in mice. Hum Gene Ther 2000;11:2493–513.
[43] Meyer O, Schughart K, Pavirani A, Kolbe HV. Multiple systemic expression of human interferon-beta in mice can be achieved upon repeated administration of optimized pcTG90-lipoplex. Gene Ther 2000;7:1606–11.
[44] Donnelly JJ, Wahren B, Liu MA. DNA vaccines: progress and challenges. J Immunol 2005;175:633–9.
[45] Rice J, Ottensmeier CH, Stevenson FK. DNA vaccines: precision tools for activating effective immunity against cancer. Nat Rev Cancer 2008;8:108–20.
[46] Cook-Mills JM, Deem TL. Active participation of endothelial cells in inflammation. J Leukoc Biol 2005;77:487–95.
[47] Kolios G, Valatas V, Kouroumalis E. Role of Kupffer cells in the pathogenesis of liver disease. World J Gastroenterol 2006;12:7413–20.
[48] Higuchi Y, Kawakami S, Yamashita F, Hashida M. The potential role of fucosylated cationic liposome/NFkappaB decoy complexes in the treatment of cytokine-related liver disease. Biomaterials 2007;28:532–9.
[49] Wong J, Kubes P, Zhang Y, Li Y, Urbanski SJ, Bennett CF, et al. Role of ICAM-1 in chronic hepatic allograft rejection in the rat. Am J Physiol Gastrointest Liver Physiol 2002;283:196–203.

Published OnlineFirst July 14, 2010; DOI:10.1158/0008-5472.CAN-10-0184

AACR

Cancer Research

Circadian Rhythm of Transferrin Receptor 1 Gene Expression Controlled by c-Myc in Colon Cancer –Bearing Mice

Fumiyasu Okazaki, Naoya Matsunaga, Hiroyuki Okazaki, et al.

Cancer Res 2010;70:6238-6246. Published OnlineFirst July 14, 2010.

Published OnlineFirst July 14, 2010; DOI:10.1158/0008-5472.CAN-10-0184

Molecular and Cellular Pathobiology

Cancer Research

Circadian Rhythm of Transferrin Receptor 1 Gene Expression Controlled by c-Myc in Colon Cancer–Bearing Mice

Fumiyasu Okazaki[1], Naoya Matsunaga[1], Hiroyuki Okazaki[1], Naoki Utoguchi[2], Ryo Suzuki[2], Kazuo Maruyama[2], Satoru Koyanagi[1], and Shigehiro Ohdo[1]

Abstract

The abundance of cell surface levels of transferrin receptor 1 (TfR1), which regulates the uptake of iron-bound transferring, correlates with the rate of cell proliferation. Because TfR1 expression is higher in cancer cells than in normal cells, it offers a target for cancer therapy. In this study, we found that the expression of TfR1 in mouse colon cancer cells was affected by the circadian organization of the molecular clock. The core circadian oscillator is composed of an autoregulatory transcription-translation feedback loop, in which CLOCK and BMAL1 are positive regulators and the *Period* (*Per*), *Cryptochrome* (*Cry*), and *Dec* genes act as negative regulators. TfR1 in colon cancer–bearing mice exhibited a 24-hour rhythm in mRNA and protein levels. Luciferase reporter analysis and chromatin immunoprecipitation experiments suggested that the clock-controlled gene *c-MYC* rhythmically activated the transcription of the *TfR1* gene. Platinum incorporation into tumor DNA and the antitumor efficacy of transferrin-conjugated liposome-delivered oxaliplatin could be enhanced by drug administration at times when TfR1 expression increased. Our findings suggest that the 24-hour rhythm of TfR1 expression may form an important aspect of strategies for TfR1-targeted cancer therapy. *Cancer Res; 70(15); 6238–46. ©2010 AACR.*

Introduction

In mammals, the master pacemaker controlling the circadian rhythm is located in the suprachiasmatic nuclei of the hypothalamus (1). Regulation of circadian physiology relies on the interplay of interconnected transcription-translation feedback loops. The BMAL1/CLOCK complex activates clock-controlled genes, including *Per*, *Cry*, and *Dec*, the products of which act as repressors by interacting with BMAL1/CLOCK (2–5). This mechanism also regulates the 24-hour rhythm in output physiology through the periodic activation/repression of clock-controlled output genes in healthy peripheral tissue and tumor tissue (6, 7).

Transferrin receptor 1 (TfR1) is involved in the uptake of iron into cells through the binding and internalization of transferrin, and its regulation by intracellular iron levels has assisted in the elucidation of many important aspects of cellular iron homeostasis (8, 9). Iron is important for metabolism, respiration, and DNA synthesis. Thus, TfR1 is expressed not only in normal healthy cells but also in malignant tumor cells (8, 10). Recently, another TfR-like molecule named TfR2 has been recognized and investigated (11, 12), but the exact function of TfR2 remains unclear (8). It has been reported that the expression of TfR1 in mammary epithelial cells exhibits a significant 24-hour rhythm (13). Such rhythmic variation in TfR1 expression seems to affect its iron uptake function resulting in time-dependent changes in the internalization of iron-loaded Tf. However, it is not clear if the expression of TfR1 in colon cancer cells shows a significant 24-hour rhythm.

Many of the pharmacologic properties of conventional drugs can be improved through the use of an optimized drug delivery system (DDS), which includes particular carriers composed primarily of lipids and/or polymers (14). The high expression of TfR1 in tumor can potentially be used to deliver cytotoxic agents into malignant cells, including chemotherapeutic drugs, cytotoxic proteins (8), and Tf-coupled polyethylene glycol (Tf-PEG) liposomes were designed as intracellular targeting carriers for drugs by systemic administration. In fact, Tf-PEG liposomes encapsulating a platinum (Pt)-based anticancer drug, oxaliplatin, can increase its accumulation in tumor masses (15, 16). On the other hand, daily rhythmic variations in biological functions are thought to affect the efficacy and/or toxicity of drugs: a large number of drugs cannot be expected to have the same potency at different administration times (7, 17). However, it is unclear what influence the rhythmic expression of TfR1 has on the pharmacokinetics/pharmacodynamics of transferrin targeting liposomes.

Authors' Affiliations: [1]Department of Pharmaceutics, Graduate School of Pharmaceutical Sciences, Kyushu University, Fukuoka, Japan and [2]Department of Pharmaceutics, Teikyo University, Sagamiko, Sagamihara, Japan

Note: Supplementary data for this article are available at Cancer Research Online (http://cancerres.aacrjournals.org/).

F. Okazaki, N. Matsunaga, and S. Ohdo contributed equally to this work.

Corresponding Author: Shigehiro Ohdo, Department of Pharmaceutics, Graduate School of Pharmaceutical Sciences, Kyushu University, Fukuoka, 812-8582, Japan. Phone: 81-92-642-6610; Fax: 81-92-642-6614; E-mail: ohdo@phar.kyushu-u.ac.jp.

doi: 10.1158/0008-5472.CAN-10-0184

Published OnlineFirst July 14, 2010; DOI:10.1158/0008-5472.CAN-10-0184

In this study, we found that the circadian expression of *c-Myc*, which is controlled by the circadian clock, affects *TfR1* gene transcription in colon cancer cells. The levels of *TfR1* mRNA and protein exhibited a 24-hour oscillation in tumor cells implanted in mice. Thus, to evaluate the rhythmic function of TfR1 and the utility for TfR1-targeting cancer therapy, we investigated how the rhythmic variation in TfR1 production influenced the pharmacologic efficacy of TfR1-targeting liposomal DDS.

Materials and Methods

Animals and cells

Seven-week-old male BALB/c mice (Charles River Japan) were housed with lights on from 7:00 a.m. to 7:00 p.m. at a room temperature of 24 ± 1°C and a humidity of 60 ± 10% with food and water *ad libitum*. Colon 26 cells (Cell Resource Center for Biomedical Research, Tohoku University) were maintained in RPMI 1640 supplemented 10% fetal bovine serum (FBS) at 37°C in a humidified 5% CO_2 atmosphere. A 25-μL volume with 2×10^7 viable tumor cells was inoculated into the right hind footpad of each mouse. The tumor volume was estimated according to a formula that has been described previously (7). Tissue slices of the removed tumor masses were made, and the tumor tissue was confirmed histopathologically.

Experimental design

To assess the temporal expression profile of TfR1 in tumor cells, tumor masses were removed from individual tumor-bearing mice at six different time points (9:00 a.m., 1:00 p.m., 5:00 p.m., 9:00 p.m., 1:00 a.m., and 5:00 a.m.) 7 days after the implantation of tumor cells. The levels of *TfR1* protein and mRNA were measured by Western blotting analysis and quantitative reverse transcription-PCR (RT-PCR), respectively. To investigate how the rhythmic variation in *TfR1* expression occurs in tumor cells, the influence of CLOCK/BMAL1 and c-MYC on the transcriptional activity of the *TfR1* gene was assessed using luciferase reporter constructs containing wild-type E-box or mutated E-box of the mouse *TfR1* promoter, which was based on previous reports. To elucidate the role of c-MYC in the control of the rhythmic expression of *TfR1*, endogenous c-MYC in Colon 26 cells was downregulated by small interfering RNA (siRNA). The c-MYC–downregulated cells were treated with 50% FBS for 2 hours to synchronize their circadian clock, and the mRNA levels of *TfR1* were assessed at 44, 48, 52, 56, 60, 64, and 68 hours after 50% serum treatment. In the same manner as described above, the protein levels of c-MYC and CLOCK were assessed by Western blotting analysis. To explore the temporal binding of endogenous c-MYC and CLOCK to the E-box in the mouse *TfR1* gene, chromatin immunoprecipitation analysis was performed in individual tumor masses at 9:00 a.m. and 9:00 p.m. To investigate the function of the 24-hour oscillation of TfR1 expression, time-dependent changes in Pt internalization into tumor cells were assessed using Tf-coupled liposomes encapsulating oxaliplatin (Tf-NGPE L-OHP). The cultured Colon 26 cells were treated with 50% FBS as described above and then harvested for RNA extraction at 0, 6, 12, 18, and 24 hours after 50% FBS treatment. Nontreated Colon 26 cells harvested at the same time points were used as the control. At 6 or 18 hours after serum treatment, cells were exposed to Tf-NGPE L-OHP (L-OHP, 0.4 mg/mL) for 3 hours. The Pt content in the DNA was measured using an inductively coupled plasma mass spectrometer (ICP-MS). To explore the dosing time–dependent difference in the internalization of Pt into tumor cells *in vivo*, tumor-bearing mice were injected with a single dose of Tf-NGPE L-OHP at 9:00 a.m. or 9:00 p.m. Plasma and tumor DNA samples were collected only once from individual mice at 1, 3, and 6 hours after injection. The plasma concentration of Pt and its content in tumor DNA were measured as described above. Then, tumor volumes were measured throughout the duration of the experiment.

RT-PCR analysis

Total RNA was extracted using RNAiso (TaKaRa). The cDNAs of mouse *TfR1* (NM011638), *TfR2* (NM015799), *c-Myc* (NM010849), and β-*actin* (NM007393) were synthesized using PrimeScript Reverse Transcriptase (TaKaRa), and the synthesized cDNAs were amplified using GoTaq Green Master Mix (Promega). The PCR products were run on 2% agarose gels. After staining with ethidium bromide, the gel was photographed using Polaroid-type film. The density of each band was analyzed using NIH image software on a Macintosh computer. To evaluate the quantitative reliability of RT-PCR, kinetic analysis of the amplified products was performed to ensure that signals were derived only from the exponential phase of amplification, as previously described (7, 17). We evaluated the validity of our semiquantitative PCR methods using real-time PCR. cDNA was prepared by reverse transcription of total RNA. Real-time PCR analysis was performed on diluted cDNA samples with SYBR Premix Ex Taq Perfect Real-Time (TaKaRa) using a 7500 Real-time PCR system (Applied Biosystems). In addition, as confirmation of RNA extraction from each tumor cell sample, the expression level of *Vegf* mRNA was measured (Supplementary Data S1).

Western blotting analysis

Nuclear or cytoplasmic proteins in tumor masses were extracted using NE-PER Nuclear and Cytoplasmic Extraction Reagents (Pierce Biotechnology). The protein concentrations were determined using a BCA Protein Assay kit (Pierce Biotechnology). The lysate samples were separated on 6% or 10% SDS-polyacrylamide gels and transferred to polyvinylidene difluoride membranes. The membranes were reacted with antibodies against TfR1 (Zymed Laboratories), c-MYC, CLOCK, β-actin (Santa Cruz Biotechnology), or RNA pol II (Abcam). The immunocomplexes were further reacted with horseradish peroxidase–conjugated secondary antibodies and visualized using Super Signal Chemiluminescent Substrate (Pierce Biotechnology). The membranes were photographed using Polaroid-type film, and the density of each band was analyzed using NIH image software on a Macintosh computer.

Published OnlineFirst July 14, 2010; DOI:10.1158/0008-5472.CAN-10-0184

Construction of reporter and expression vectors

The 5′ flanking region of mouse *TfR1* (from bp +16 to +436; +1 indicates the transcription start site) gene was amplified using Elongase Enzyme mix (Invitrogen) using DNA extracted from Colon 26 cells. PCR was performed using the forward primer 5′-AGTTGAGCTC(*Sac*I)GGCTTGGTGCAGCTCAGTTAGTAG-3′ and reverse primer 5′-ATGAGATATC(*Eco*RV)TAAATGTCCGTTGACACTAGTAACC-3′. The PCR products were purified and ligated into a pGL4 Basic vector (*Tf*R1-Luc). The sequence of the CACGTG E-box (bp +290 to +295) on *Tf*R1-Luc was mutated using a QuikChange site-directed mutagenesis kit (Stratagene). Expression vectors for mouse CLOCK, BMAL1, and c-Myc were constructed using cDNAs obtained from RT-PCR derived from mouse liver RNA. All coding regions were ligated into the pcDNA3.1 (+) vector (Invitrogen), as previously described (7). Protein expression levels from each expression vector in Colon 26 were assessed by Western blotting analysis (Supplementary Data S2).

Luciferase reporter assay

Colon 26 cells were seeded at 3×10^5 cells per well in six-well culture plates (BD Biosciences). After an 18-hour culture, the cells were transfected with 100 ng per well of reporter vector and 2 μg per well (total) of expression vector using Lipofectamine LTX reagent (Invitrogen). A 0.5-ng-per-well sample of phRL-TK vector (Promega) was also cotransfected as an internal control reporter. The total amount of DNA per well was adjusted by adding pcDNA3.1 vector (Invitrogen). At 24 hours posttransfection, cells were harvested and the cell lysate was analyzed using a dual-luciferase reporter assay system (Promega). The ratio of firefly luciferase activity to *Renilla* luciferase activity in each sample served as a measure of normalized luciferase activity.

Small interfering RNA

siRNA of the mouse *c-Myc* gene was designed using BLOCK-iT RNAi Designer (Invitrogen). The siRNA oligonucleotide sequences were as follows: siRNA control sense, 5′-UAGUGUGAGCACUGUGAUUCCUUGG-3′ and antisense 5′-CCAAGGAUCACAGUGCUCACACUA-3′; *c-Myc* siRNA sense 5′-UAGUCGAGGUC-AUAGUUCCUGUUGG-3′ and antisense 5′-CCAACAGGAACUAUGACCUCGACUA-3′. The oligonucleotides were transfected into Colon 26 cells at a final concentration of 20 nmol/L using Lipofectamine 2000 (Invitrogen).

Chromatin immunoprecipitation assays

Tumor masses were excised and treated with 1% formaldehyde for 5 minutes at room temperature to cross-link the chromatin, and the reaction was stopped by adding glycine to a final concentration of 0.125 mol/L. Each cross-linked sample was sonicated on ice and then incubated with antibodies against c-MYC, CLOCK, rabbit-IgG, or goat-IgG (Santa Cruz Biotechnology). Chromatin/antibody complexes were extracted using a protein G agarose kit (Roche). DNA was isolated using the Wizard SV Genomic DNA Purification System (Promega) and subjected to PCR using the following primers for the c-MYC binding site (E-box) of the *TfR1* promoter region, forward 5′-GTGACTCCCTTGTCAG-3′ and reverse 5′-CCGTGACACTAGTAACC-3′. For PCR analysis, PCR products were amplified for 40 or 45 cycles. PCR products were run on an agarose (3%) gel, including 0.2 μg/mL ethidium bromide, and analyzed using the NIH image software.

Determination of L-OHP (Pt) concentration

Plasma samples were obtained by centrifugation at 3,000 rpm for 3 minutes and stored at −20°C until analysis. Tumor DNA was extracted using a Wizard Genomic DNA Purification kit (Promega). Measurements of the L-OHP (Pt) content in plasma and tumor DNA were made using ICP-MS at the Center of Advanced Instrumental Analysis, Kyushu University. ICP-MS is capable of detecting very small amounts of Pt. Plasma Pt concentration and its tumor DNA content were expressed as micrograms per milliliter and nanograms per nanogram of DNA, respectively.

Determination of the antitumor effect

Seven days after the inoculation of Colon 26 cells into mice, a single injection of Tf-NGPE L-OHP (L-OHP: 0, 7.5 mg/kg, i.v.) or vehicle (9% sucrose) was given to tumor-bearing mice at 9:00 a.m. or 9:00 p.m. This dosage of Tf-NGPE L-OHP was selected based on a preliminary study (Supplementary Data S3). In all mice, the tumor volumes were measured every 3 days throughout the duration of the experiment.

Statistical analysis

ANOVA was used for multiple comparisons, and Scheffe's test was used for comparison between two groups. A 5% level of probability was considered significant.

Results

Twenty-four-hour rhythm in the expression of TfR1 in Colon 26 tumor masses

Two subtypes of TfR have been identified: TfR1 and TfR2. In implanted Colon 26 cells, *TfR1* but not *TfR2* was detectable, although *TfR2* was expressed in mouse liver (Supplementary Data S1B). The protein and mRNA levels of TfR1 in implanted Colon 26 cells showed a significant 24-hour rhythm, with higher levels during the early dark phase ($P < 0.05$; Fig. 1A and B). The increase and decrease in mRNA levels of *TfR1* seemed to cause the rhythm of TfR1 protein in Colon 26 tumor masses.

Regulation of the 24-hour rhythm in the expression of *TfR1* gene by c-MYC

Among these, c-MYC is a potent activator of *TfR1* gene transcription in mice and humans, and the transactivation effect was elicited through binding to the CACGTG E-box located in the first intron region (18, 19). In addition, CLOCK/BMAL1 heterodimers also bind cooperatively to CACGTG E-box sequences and regulate the rhythmic expression of their target genes (2). Thus, to establish the relevance of the biological clock system on the expression of *TfR1*, CLOCKΔ19 (CLOCK protein lacking transcriptional activity) was overexpressed in Colon 26 cells. Clock mutant mice have

Published OnlineFirst July 14, 2010; DOI:10.1158/0008-5472.CAN-10-0184

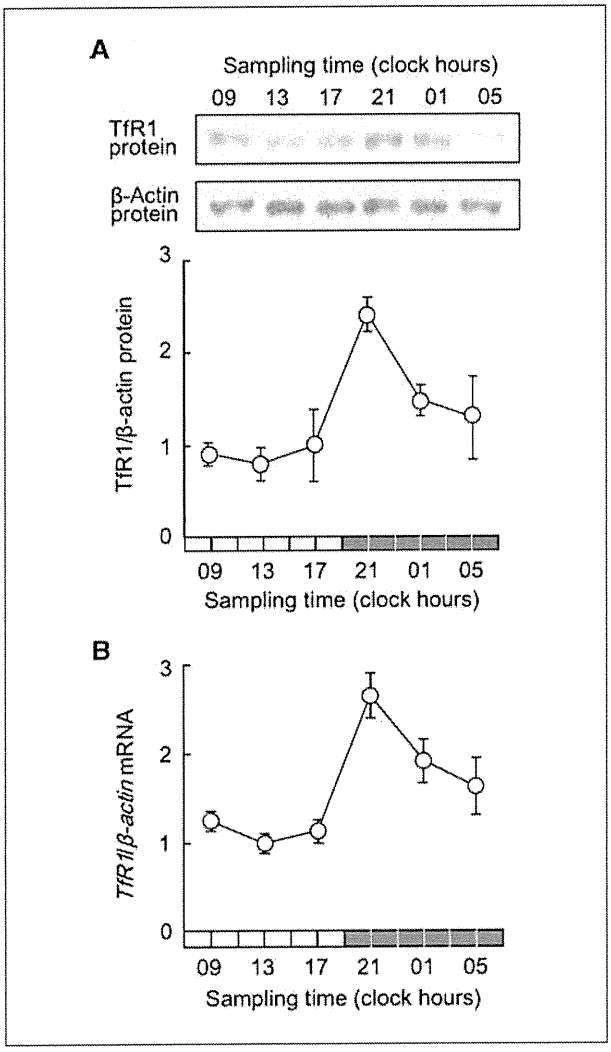

Figure 1. Twenty-four hour variation in the expression of TfR1 in Colon 26 tumor masses. A, temporal expression profile of TfR1 protein in tumor masses. The photographs show 24-h variation in TfR1 protein in implanted Colon 26 tumor cells. Cytoplasmic proteins were measured using each of the antibodies. Bottom, relative TfR1 protein levels. The data were normalized using β-actin as a control. Points, mean (n = 3, P < 0.01, ANOVA); bars, SEM. B, temporal expression profile of *TfR1* mRNA in tumor masses. The data are normalized using β-*actin* as a control. Points, mean (n = 6, P < 0.01, ANOVA); bars, SEM.

a point mutation in exon 19 of the *Clock* gene and exhibit low-amplitude rhythms in the expression of various genes (20). *TfR1* and *c-Myc* expression levels were low in CLOCKΔ19 overexpressing Colon 26 cells (Supplementary Data S4). Next, we tested whether these transcription factors participate in regulation of the rhythmic expression of *TfR1* gene in Colon 26 cells. Cotransfection of *TfR1*-Luc with c-MYC expression constructs resulted in an 8.1-fold increase in promoter activity, whereas CLOCK/BMAL1 had little effect on the transcriptional activity of the *TfR1* gene (Fig. 2B). The transactivation effect of c-MYC on *TfR1* reporters was dependent on the E-box element located from bp +290 to +295 because mutation of the CACGTG sequence to AAGCTT reduced transcriptional activation by c-MYC from 8.1- to 1.5-fold.

Several compounds and high concentration serum have been shown to induce and/or synchronize circadian gene expression in cultured cells (21). Thus, to elucidate the role of c-MYC in the circadian regulation of *TfR1* expression, the temporal expression profiles of *TfR1* mRNA in c-MYC–downregulated Colon 26 cells were investigated after 50% FBS treatment. Brief exposure of control scrambled siRNA-transfected cells to 50% FBS resulted in the oscillation of *TfR1* mRNA levels with a period length of ~24 hours (Fig. 3A). On the other hand, the protein levels of c-MYC were decreased and the mRNA levels of *TfR1* failed to show a significant 24-hour oscillation after the treatment of *c-Myc* siRNA–transfected cells with 50% FBS (Fig. 3B and C). These results suggested that c-MYC is required for generating the time-dependent variation in *TfR1* mRNA expression.

The transcription of *c-Myc* is regulated by components of the circadian clock, and its mRNA levels in mouse liver and bones have been shown to exhibit a significant 24-hour oscillation (22). The protein levels of c-MYC in Colon 26 cells implanted in mice also showed obvious 24-hour oscillations with higher levels around the early dark phase and lower levels during the early light phase, whereas there was no obvious 24-hour variation in the protein levels of CLOCK in the tumor

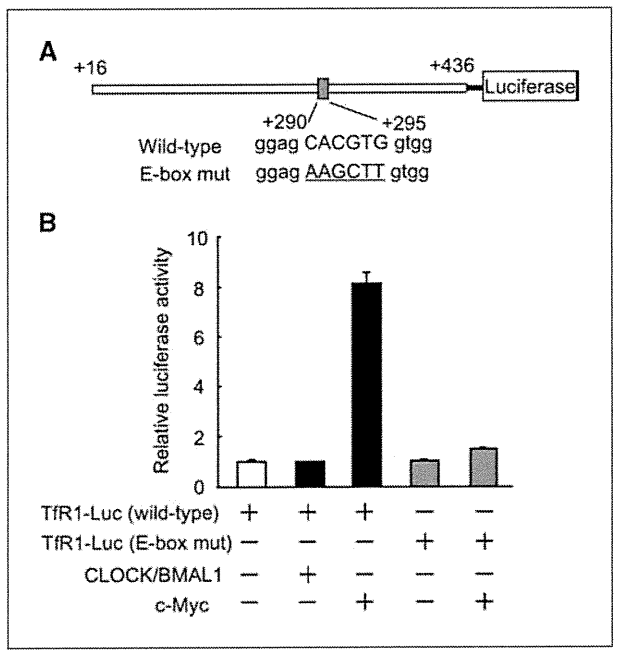

Figure 2. Influence of CLOCK/BMAL1 and c-MYC on transcription of the mouse *TfR1* gene. A, schematic representation of the mouse *TfR1* promoter. The numbers on both sites, the distance (bp) from the transcription start site (+1) included in the luciferase reporter construction. The numbers of nucleotide residues below the box, the positions of the E-box. The underlined nucleotide residues, the mutated sequence of the E-box. B, wild-type or E-box–mutated *TfR1* gene reporter plasmids (*TfR1*-Luc) were cotransfected with expression constructs encoding CLOCK/BMAL1 or c-MYC. Columns, mean (n = 3); bars, SEM.

Published OnlineFirst July 14, 2010; DOI:10.1158/0008-5472.CAN-10-0184

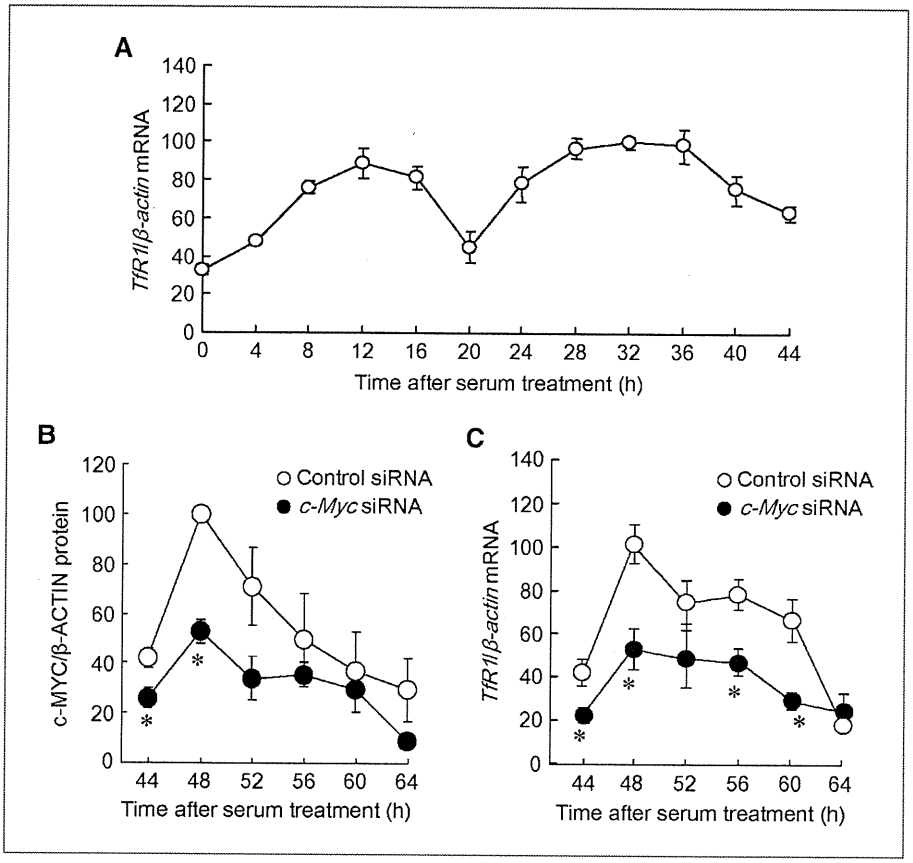

Figure 3. Influence of the downregulation of c-MYC on the rhythmic expression of *TfR1* mRNA in Colon 26 cells. A, temporal accumulation of *TfR1* mRNA in Colon 26 cells after 50% serum shock. The data are normalized using β-*actin* as a control. Points, mean ($n = 3$, $P < 0.01$, ANOVA); bars, SEM. Data are plotted relative to the 0-h value after 50% serum shock. B, temporal accumulation of c-MYC protein in control cells or c-Myc knockdown cells after 50% serum shock. Colon 26 cells were transfected with scrambled siRNA (control siRNA) or specific siRNA for c-Myc (c-Myc siRNA). Crude cell extracts were measured by Western blotting analysis. The data were normalized using β-actin as a control. Points, mean ($n = 3$, control cells; $P < 0.01$, ANOVA); bars, SEM. *; $P < 0.05$, when compared with the value for the control siRNA group at the corresponding times. C, temporal accumulation of *TfR1* mRNA in control cells or *c-Myc* knockdown cells. The mRNA levels of *TfR1* were determined at the indicated time points after serum treatment. Points, mean ($n = 3$, control cells; $P < 0.01$, ANOVA); bars, SEM. *, $P < 0.05$, when compared with the value for the control siRNA group at the corresponding times.

cells (Fig. 4A). The results of chromatin immunoprecipitation analysis revealed that endogenous c-MYC in Colon 26 cells bound to the E-box element in the intron region of *TfR1* gene (Fig. 4B). Of particular note, the binding amounts of c-MYC increasedat the time of day corresponding to the peak of *TfR1* mRNA expression (see Fig. 1B), suggesting that the time-dependent binding of c-MYC to the E-box in *TfR1* gene underlies its rhythmic expression. In addition, the mRNA levels of a prototypical c-MYC–regulated gene, telomerase reverse transcriptase (23), in Colon 26 cells implanted in mice also showed time-dependent variation (Supplementary Data S5).

Relationship between the rhythmic expression of TfR1 and time dependency of Pt incorporation into tumor DNA

Tf-NGPE L-OHP is a transferrin-conjugated liposome encapsulating L-OHP, a diaminocyclohexane Pt antitumor agent, which forms adducts with DNA. Tf-NGPE L-OHP binds to TfR, which is expressed on the plasma membrane and can internalize Pt into the cell.[3] Thus, to explore the function of internalization into the cell through transferrin in the rhythmic expression of TfR1, we investigated the temporal profile of *TfR1* gene expression and incorporation of Pt into tumor DNA in synchronized and desynchronized Colon 26 cells. A brief exposure of cultured Colon 26 cells to 50% FBS medium for 2 hours induced an oscillation in the expression of *TfR1* mRNA (Fig. 5A). The mRNA levels of *TfR1* peaked at 18 hours after treatment of the cells with 50% FBS. The oscillation of *TfR1* mRNA levels was also found on day 3 after serum treatment (see Fig. 3). The amount of Pt incorporated into the DNA of serum-shocked cells after treatment with Tf-NGPE L-OHP increased significantly at the time point corresponding to the peak in the level of TfR1 protein ($P < 0.05$; Fig. 5B). In contrast, in nontreated cells, neither the mRNA and protein levels of TfR1 nor Pt incorporation showed significant time-dependent variations (Fig. 5A and B), suggesting that the oscillation in the

[3] Our unpublished data.

Published OnlineFirst July 14, 2010; DOI:10.1158/0008-5472.CAN-10-0184

expression of TfR1 underlies the time-dependent change in Pt incorporation into tumor DNA.

Influence of dosing time on the ability of Tf-NGPE L-OHP to inhibit tumor growth

The plasma Pt concentration decreased gradually after a single injection of 7.5 mg/kg Tf-NGPE L-OHP (i.v.) at both dosing times, but the Pt concentration in plasma at 3 hours after Tf-NGPE L-OHP injection was significantly higher in mice injected with the drug at 9:00 a.m. than at 9:00 p.m. (Fig. 6A, left). On the other hand, Pt incorporation into DNA in tumor cells at 3 and 6 hours after Tf-NGPE L-OHP injection was significantly higher in mice injected with the drug at 9:00 p.m. than at 9:00 a.m. (Fig. 6A, right). We also attempted to determine the Pt contents in tumor DNA at over 6 hours after Tf-NGPE L-OHP injection, but accurate assessment was difficult, probably due to L-OHP–induced apoptotic or necrotic tumor cell death.

A significant antitumor effect of Tf-NGPE L-OHP was observed when tumor-bearing mice were injected i.v. with a single dose of 7.5 mg/kg L-OHP (Supplementary Data S3). Thus, the dosage was set at 7.5 mg/kg to investigate whether the antitumor effect of Tf-NGPE L-OHP was altered depending on its dosing time. The growth of tumor cells was significantly suppressed by the administration of Tf-NGPE L-OHP (7.5 mg/kg, i.v.). The antitumor effects were more potent in mice injected with the drug at 9:00 p.m. than in those that received it at 9:00 a.m. (Fig. 6B). Fifteen days after injection of the drug, the tumor volume in mice injected with Tf-NGPE L-OHP at 9:00 p.m. was significantly smaller than that in mice injected at 9:00 a.m. ($P < 0.05$).

Discussion

TfR1 is a key cell surface molecule that regulates the uptake of iron-bound transferrin (8). It has been shown that correlation exists between the number of surface TfR1 and the rate of cell proliferation. TfR1 expression is higher in tumor cells than in normal cells. Thus, intracellular targeting using iron-saturated Tf as a ligand for TfR-mediated endocytosis has attracted attention. In this study, the protein abundance of TfR1 on Colon 26 tumor cells implanted in mice showed a clear 24-hour oscillation. The rhythmic phase of TfR1 protein

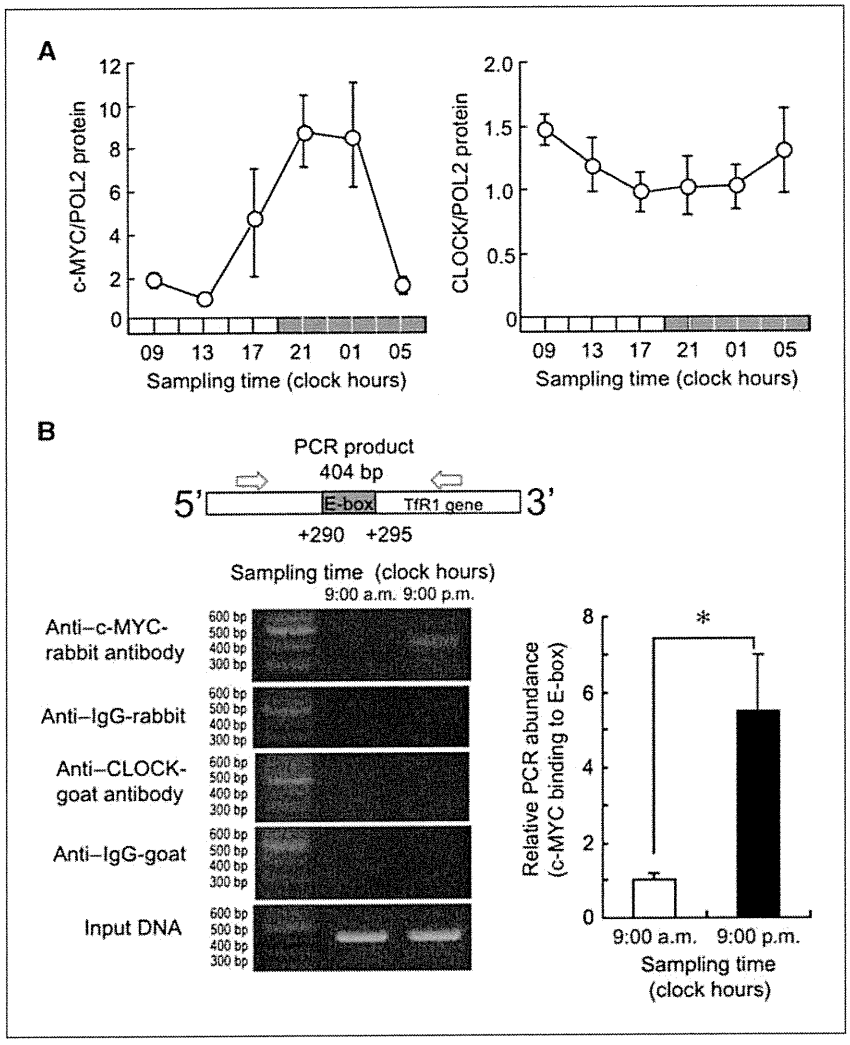

Figure 4. Time-dependent changes in the binding of endogenous c-MYC to the E-box element in the *TfR1* gene. A, temporal expression profiles of protein levels of c-MYC and CLOCK in implanted Colon 26 tumor masses. POL2 protein was used as an internal control whose expression was constant throughout the day. The data are normalized using POL2 as a control ($P < 0.01$, ANOVA). CLOCK protein did not show an obvious variation. Points, mean ($n = 3$); bars, SEM. B, left, temporal profiles of the binding of endogenous c-MYC to the *TfR1* gene in Colon 26 cells implanted in mice. Right, the quantification of temporal changes in the binding of c-MYC to the *TfR1* gene in Colon 26 cells implanted in mice. The mean value of each assay at 9:00 a.m. was set at 1. Columns, mean ($n = 3$); bars, SEM. *; $P < 0.05$ for the comparison between the two groups.

Published OnlineFirst July 14, 2010; DOI:10.1158/0008-5472.CAN-10-0184

paralleled that of its mRNA levels. However, the mechanisms of transcriptional rhythm of TfR1 were unclear.

The molecular circadian clock operates at a cellular level and coordinates a wide variety of physiologic processes (24). CLOCK/BMAL1 heterodimers activate the transcription of *Per*, *Cry*, and *Dec* genes through CACGTG E-box enhancer elements (8). The results of luciferase reporter assays and chromatin immunoprecipitation experiments revealed that the CACGTG E-box located in the first intron of the mouse *TfR1* gene was unable to respond to CLOCK/BMAL1 heterodimers. In contrast, as reported previously (19), c-MYC could bind to the E-box of the mouse *TfR1* gene and activate its transcription. The amount of endogenous c-MYC protein binding to the mouse *TfR1* gene E-box fluctuated in a time-dependent manner. The binding of c-MYC to the E-box increased at the time corresponding to the peak of *TfR1* mRNA expression, suggesting that c-MYC acts as a regulator of circadian expression of the *TfR1* gene in Colon 26 tumor cells. This hypothesis was also supported by the present findings that the amplitude of the *TfR1* mRNA rhythm in serum-shocked Colon 26 cells was decreased by the down-regulation of c-MYC. On the other hand, CLOCK protein did not bind to the *TfR1* gene E-box. This may account for the unresponsiveness of the *TfR1* gene to CLOCK/BMAL1 heterodimers. The sequence surrounding the E-box and its location had a marked influence on the transcriptional activity of CLOCK/BMAL1 (6). In fact, a CT-rich *cis*-acting element of the mouse vasopressin gene confers robust CLOCK/BMAL1 responsiveness on an adjacent E-box (25). The absence of such a CT-rich *cis*-acting element around the E-box may result in the inability of CLOCK/BMAL1 to transactivate the mouse *TfR1* gene.

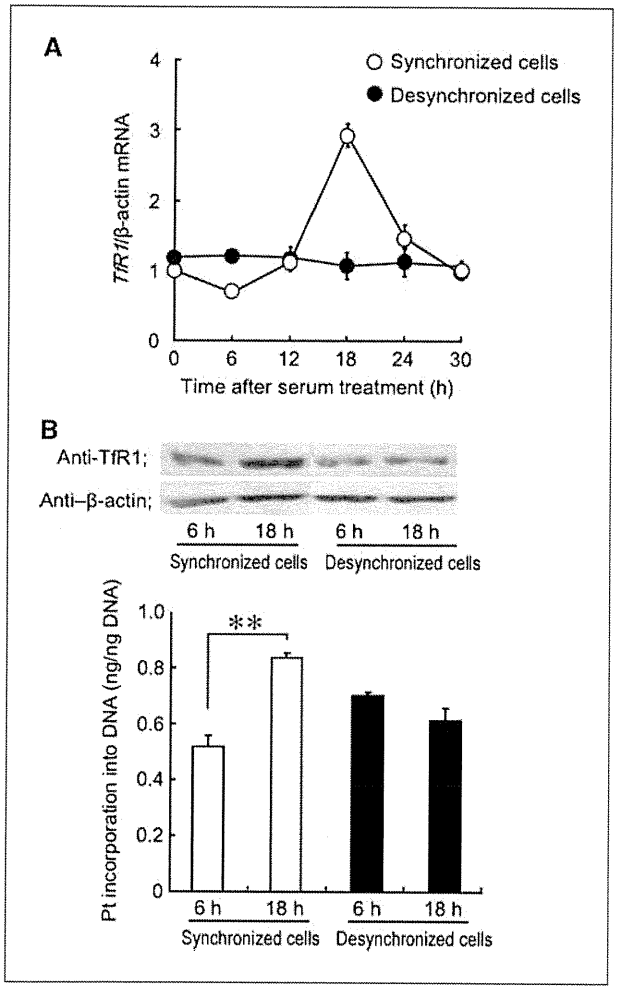

Figure 5. Influence of rhythmic changes in the expression of TfR1 on intratumoral delivery of L-OHP by Tf-NGPE liposomes. A, the temporal expression profile of *TfR1* mRNA in synchronized (○) or unsynchronized (•) Colon 26 cells. Cultured Colon 26 cells were synchronized by exposure to 50% FBS for 2 h. Points, mean (n = 3, synchronized cells; $P < 0.05$, ANOVA); bars, SEM. B, the photographs show temporal expression of TfR1 protein in synchronized or unsynchronized Colon 26 cells. Bottom, that temporal profile of Pt incorporation into DNA in synchronized or unsynchronized Colon 26 cells. Cells were exposed to Tf-NGPE L-OHP (L-OHP: 0.4 mg/mL) for 3 h at 6 or 18 h after the serum treatment, and then the amounts of Pt incorporated into tumor DNA were measured. Columns, mean (n = 3); bars, SEM. *, $P < 0.05$ for the comparison between the two time points.

Because the rhythmic phase of c-MYC protein abundance in Colon 26 cells correlated with the time dependency of its binding to the *TfR1* gene E-box, the oscillation in c-MYC protein levels may cause the 24-hour rhythm in the expression of downstream genes by rhythmic binding to their DNA response elements. In fact, *mTERT* mRNA in implanted Colon 26 tumor also showed time-dependent variation. In addition, *c-Myc* is regulated by clock genes, as indicated by previous results (26). *TfR1* and *c-Myc* expression levels were low in CLOCKΔ19-overexpressing Colon 26 cells. Although the E-box of the *TfR1* gene did not respond to CLOCK/BMAL1, the molecular components of the circadian clock may indirectly regulate the expression of the *TfR1* gene in Colon 26 cells.

It was reported previously that L-OHP could accumulate in tumor masses following delivery using Tf-PEG liposomes (16). TfR-targeting liposomes also bind to TfR on tumor cell surfaces and are internalized into the cells by receptor-mediated endocytosis. In this study, to evaluate the function of the 24-hour oscillation in TfR1, Tf-NGPE liposomes were used as a targeting carrier for intratumoral delivery of L-OHP. This TfR-targeting liposomal DDS exhibited similar pharmacokinetic properties to Tf-PEG liposomes, and i.v. administration of L-OHP encapsulated within Tf-NGPE liposomes lead to the accumulation of a high concentration of L-OHP in tumors as much as Tf-PEG liposomes.[4] The amount of Pt in tumor DNA after Tf-NGPE L-OHP injection increased at the times of day when TfR1 was abundant on the tumor surface in this study. This notion was also supported by *in vitro* findings that the time dependency of Tf-NGPE liposome–delivered L-OHP into tumor cells disappeared in the absence of the oscillation in TfR1 expression. These findings suggest that the oscillation in the expression of TfR1 underlies the dosing time–dependent changes in the internalization into

[4] Our unpublished data.

Published OnlineFirst July 14, 2010; DOI:10.1158/0008-5472.CAN-10-0184

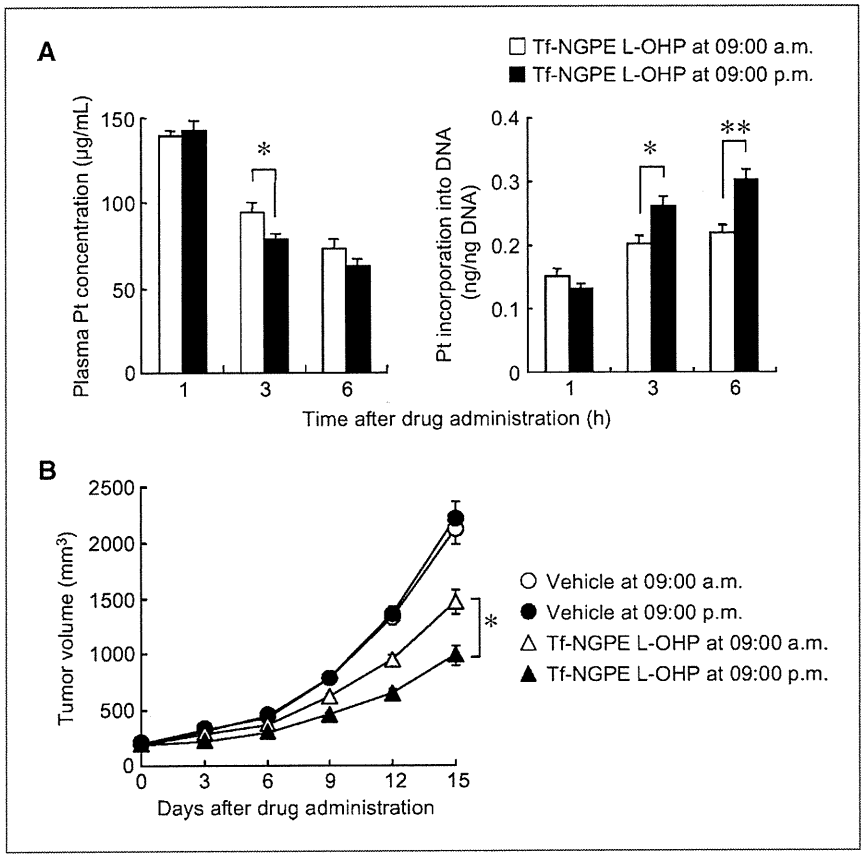

Figure 6. Influence of dosing time on the ability of Tf-PEG L-OHP to inhibit tumor growth in mice. Colon 26 tumor–bearing mice were injected i.v. with a single dose of Tf-NGPE L-OHP (L-OHP: 7.5 mg/kg) or vehicle (9% sucrose) at 9:00 a.m. or 9:00 p.m. A, dosing time–dependent differences in the intratumoral delivery of L-OHP by Tf-NGPE liposomes were examined. Plasma Pt concentration (left) and Pt incorporation into tumor DNA (right) were measured at the indicated times after an injection of Tf-NGPE L-OHP. Columns, mean (n = 5); bars, SEM; **, $P < 0.01$; *, $P < 0.05$ for comparison between the two groups. B, dosing time–dependent difference in the antitumor effect of Tf-NGPE L-OHP. Points, mean (n = 8–10); bars, SEM; *, $P < 0.05$ for comparison between the two dosing times.

the cells by receptor-mediated endocytosis. In addition, after a single injection of Tf-NGPE L-OHP, the antitumor effect of the drug varied according to its dosing time. The dosing time dependency of the antitumor effect seemed to be caused by time-dependent changes in the intratumoral delivery of L-OHP by TfR-targeting liposomes.

In the present study, it was shown that the 24-hour rhythm of TfR1 expression in colon cancer cells was controlled by c-MYC, and the cyclical accumulation of TfR1 caused dosing time–dependent changes in the intratumoral delivery of L-OHP by receptor-mediated endocytosis. Identification of the circadian properties of molecules that are targeted by ligand-directed DDS may aid the choice of the most appropriate time of day for their administration.

Disclosure of Potential Conflicts of Interest

The authors disclose no conflicts.

Grant Support

Grants-in-Aid for Scientific Research on Priority Areas "Cancer" (S.O. 20014016) from the Ministry of Education, Culture, Sport, Science and Technology of Japan, for Scientific Research (B; S.O. 21390047), for Challenging Exploratory Research (S.O. 21659041), and for the Encouragement of Young Scientists (N.M. 20790137) from the Japan Society for the Promotion of Science.

The costs of publication of this article were defrayed in part by the payment of page charges. This article must therefore be hereby marked *advertisement* in accordance with 18 U.S.C. Section 1734 solely to indicate this fact.

Received 01/18/2010; revised 06/07/2010; accepted 06/07/2010; published OnlineFirst 07/14/2010.

References

1. Stephan FK, Zucker I. Circadian rhythms in drinking behavior and locomotor activity of rats are eliminated by hypothalamic lesions. Proc Natl Acad Sci U S A 1972;69:1583–6.
2. Alvarez JD, Sehgal A. Circadian rhythms: finer clock control. Nature 2002;419:798–9.
3. Gekakis N, Staknis D, Nguyen HB, et al. Role of the CLOCK protein in the mammalian circadian mechanism. Science 1998;280:1564–9.
4. Kume K, Zylka MJ, Sriram S, et al. mCRY1 and mCRY2 are essential components of the negative limb of the circadian clock feedback loop. Cell 1999;98:193–205.
5. Preitner N, Damiola F, Lopez-Molina L, et al. The orphan nuclear receptor REV-ERBα controls circadian transcription within the positive limb of the mammalian circadian oscillator. Cell 2002;110:251–60.
6. Sato TK, Yamada RG, Ukai H, et al. Feedback repression is required for mammalian circadian clock function. Nat Genet 2006;38:312–9.

Published OnlineFirst July 14, 2010; DOI:10.1158/0008-5472.CAN-10-0184

7. Koyanagi S, Kuramoto Y, Nakagawa H, et al. A molecular mechanism regulating circadian expression of vascular endothelial growth factor in tumor cells. Cancer Res 2003;63:7277–83.
8. Daniels TR, Delgado T, Helguera G, Penichet ML. The transferrin receptor part II: targeted delivery of therapeutic agents into cancer cells. Clin Immunol 2006;121:159–76.
9. Sorokin LM, Morgan EH, Yeoh GC. Transformation-induced changes in transferrin and iron metabolism in myogenic cells. Cancer Res 1989;49:1941–7.
10. Niitsu Y, Kohgo Y, Nishisato T, et al. Transferrin receptors in human cancerous tissues. Tohoku J Exp Med 1987;153:239–43.
11. Calzolari A, Oliviero I, Deaglio S, et al. Transferrin receptor 2 is frequently expressed in human cancer cell lines. Blood Cells Mol Dis 2007;39:82–91.
12. Kawabata H, Nakamaki T, Ikonomi P, Smith RD, Germain RS, Koeffler HP. Expression of transferrin receptor 2 in normal and neoplastic hematopoietic cells. Blood 2001;98:2714–9.
13. Röhrs S, Kutzner N, Vlad A, Grunwald T, Ziegler S, Müller O. Chronological expression of Wnt target genes Ccnd1, Myc, Cdkn1a, TfRc, Plf1 and Ramp3. Cell Biol Int 2009;33:501–8.
14. Papahadjopoulos D, Allen TM, Gabizon A, et al. Sterically stabilized liposomes: improvements in pharmacokinetics and antitumor therapeutic efficacy. Proc Natl Acad Sci U S A 1991;88:11460–4.
15. Ishida O, Maruyama K, Tanahashi H, et al. Liposomes bearing polyethyleneglycol-coupled transferrin with intracellular targeting property to the solid tumors *in vivo*. Pharm Res 2001;18:1042–8.
16. Suzuki R, Takizawa T, Kuwata Y, et al. Effective anti-tumor activity of oxaliplatin encapsulated in transferrin-PEG-liposome. Int J Pharm 2008;346:143–50.
17. Ohdo S, Koyanagi S, Suyama H, Higuchi S, Aramaki H. Changing the dosing schedule minimizes the disruptive effects of interferon on clock function. Nat Med 2001;3:356–60.
18. Holloway K, Sade H, Romero IA, Male D. Action of transcription factors in the control of transferrin receptor expression in human brain endothelium. J Mol Biol 2007;365:1271–84.
19. O'Donnell KA, Yu D, Zeller KI, et al. Activation of transferrin receptor 1 by c-Myc enhances cellular proliferation and tumorigenesis. Mol. Cell Biol 2006;26:2373–86.
20. Oishi K, Miyazaki K, Kadota K, et al. Genome-wide expression analysis of mouse liver reveals CLOCK-regulated circadian output genes. J Biol Chem 2003;278:41519–27.
21. Takiguchi T, Tomita M, Matsunaga N, Nakagawa H, Koyanagi S, Ohdo S. Molecular basis for rhythmic expression of CYP3A4 in serum-shocked HepG2 cells. Pharmacogenet Genomics 2007;17:1047–56.
22. Wittekindt NE, Hörtnagel K, Geltinger C, Polack A. Activation of c-*myc* promoter P1 by immunoglobulin κ gene enhancers in Burkitt lymphoma: functional characterization of the intron enhancer motifs κB, E box 1 and E box 2, and of the 3′ enhancer motif PU. Nucleic Acids Res 2000;28:800–8.
23. Reymann S, Borlak J. Transcription profiling of lung adenocarcinomas of c-*myc*-transgenic mice: identification of the c-*myc* regulatory gene network. BMC Syst Biol 2008;2:46.
24. Weaver ReppertSM. Coordination of circadian timing in mammals. Nature 2002;418:935–41.
25. Muñoz E, Brewer M, Baler R. Modulation of BMAL/CLOCK/E-Box complex activity by a CT-rich *cis*-acting element. Mol Cell Endocrinol 2006;252:74–81.
26. Fu L, Pelicano H, Liu J, Huang P, Lee C. The circadian gene Period2 plays an important role in tumor suppression and DNA damage response *in vivo*. Cell 2002;111:41–50.

—Reviews—

ファージディスプレイ法を用いた腫瘍組織血管抗体の創製

山下琢矢,*,a,b,c 宇都口直樹,a 鈴木 亮,a 長野一也,b
角田慎一,b,d 堤 康央,b,c,d 丸山一雄a

Development of Anti-tumor Blood Vessel Antibodies by Phage Display Method

Takuya YAMASHITA,*,a,b,c Naoki UTOGUCHI,a Ryo SUZUKI,a Kazuya NAGANO,b
Shin-ichi TSUNODA,b,d Yasuo TSUTSUMI,b,c,d and Kazuo MARUYAMAa

aDepartment of Biopharmaceutics, School of Pharmaceutical Sciences, Teikyo University, Suarashi1091-1, Sagamiko, Sagamihara, Kanagawa 229-0195, Japan, bLaboratory of Pharmaceutical Proteomics, National Institute of Biomedical Innovation, 7-6-8 Saito-Asagi, Ibaraki, Osaka 567-0085, Japan, cThe Department of Toxicology, School of Pharmaceutical Sciences, Osaka University, 1-6 Yamadaoka, Suita, Osaka 565-0871, Japan, and dThe Center for Advanced Medical Engineering and Informatics, Osaka University, 2-2 Yamadaoka, Suita, Osaka 565-0871, Japan

(Received August 31, 2009)

Tumor blood vessels are essential for tumor growth. Therefore, these blood vessels are potential targets for anti-cancer therapy. The purpose of this study is to develop anti-tumor endothelial cell (TEC) antibodies for delivering anti-cancer agents or drugs. To achieve this goal, we utilized the phage antibody display library method to create monoclonal antibodies *in vitro*. Accordingly, we developed anti-TEC antibodies from an single chain Fv fragment (scFv) phage display library prepared using the Fv genes amplified from the mRNAs isolated from the TEC-immunized mice. The size of the phage antibody library prepared from the mRNA of the TEC-immunized mice was approximately 1.3×10^7 CFU. To select and enrich for the phages displaying the anti-TEC antibodies, cell panning was performed first using the TEC followed by subtractive panning using the normal endothelial cell. After five cycles of panning, the affinity of bound phage clones increased approximately 10 000 folds. Subsequently, clones isolated from the post-panning output library were tested for their antigen-specificity by ELISA and western blotting. One of the scFv phage clones showing antigen-specificity recognized only TEC *in vitro*, and when injected into the Colon26 bearing mice, this clone accumulated more on the tumor tissue than the wild type phage. These results suggest that the isolated an antibody and this clone's target molecule could be potentially useful for novel anti-tumor therapies.

Key words——tumor endothelial cell; phage display; antibody

1. はじめに

医療技術の進歩に伴い，各種疾患の治療成績は年々向上している一方で，「悪性新生物：がん」は1981年にわが国における死因の第1位となって以来，その死亡者は年々増加し，現在では死因全体の約3割を占めている．このように，「がん」を克服できていない現状から，新たながん治療法，診断法の確立が待望されている．

腫瘍組織は，その体積が1 mm³を超えて増大する際，血管より最も離れた中心部位は低酸素状態にある．[1-3] そして，HIF等を介してその低酸素シグナルは腫瘍細胞に伝わり，腫瘍細胞がVEGF，b-FGF等の血管新生誘導因子を産生し，新たな血管を既存の血管より誘導してくることが知られている．[4-7] この腫瘍により誘導された血管は，腫瘍細胞への酸素・栄養の供給，腫瘍細胞からの老廃物の除去という腫瘍にとってまさにライフラインとも言うべき機能をしており，腫瘍組織の維持，増大に必要不可欠である．[8,9] さらに，この腫瘍組織血管の誘導は腫瘍の増大だけでなく，腫瘍血行性転移の経路

aa帝京大学薬学部生物薬剤学教室（〒229-0195 神奈川県相模原市相模湖町1091-1），b独立行政法人医薬基盤研究所基盤的研究部創薬プロテオミクスプロジェクト（〒567-0085 大阪府茨木市彩都あさぎ7-6-8），c大阪大学大学院薬学研究科毒性学分野（〒565-0871 大阪府吹田市山田丘1-6），d大阪大学臨床医工学融合研究教育センター（〒565-0871 大阪府吹田市山田丘2-2）
*e-mail: t-yamashita@nibio.go.jp

本総説は，日本薬学会第129年会シンポジウムGS6で発表したものを中心に記述したものである．

としても機能している．このように腫瘍組織血管は腫瘍組織にとって必要不可欠な存在であるため，腫瘍組織血管に対して傷害を誘導することは腫瘍組織に致死的なダメージを与えることになり，腫瘍の退縮及び，転移の抑制が期待できる．このような背景も相まって，現在，この腫瘍組織血管を標的とするような分子標的医薬品の開発が盛んに進められている．

近年，疾患関連分子に対する分子標的治療を可能とするモノクローナル抗体が脚光を浴びている．その優れた抗原特異性から，モノクローナル抗体は診断薬[10-14]として，さらには最近，抗体医薬として応用が非常に注目され，研究，臨床開発が盛んに行われており，現在，基礎研究段階のものを含めれば，約400以上もの抗体医薬品の研究開発が進められているとされている．[15-20] また，2007年の抗体医薬品の世界市場は約263億3800万ドル（約2兆3800億円）で，2013年には約490億5500万ドル（約4兆4300億円）まで拡大すると予想され，まさに熾烈な研究合戦が世界規模で展開中である．本邦においても，乳がんにおいて過剰発現が認められるerbB2を標的とするTrastuzumab（Herceptin®），[21-23] がんの血管新生をターゲットとした抗VEGF中和抗体であるBevacizumab（Avastin®）[24,25]を始め，徐々に抗体医薬品が承認・上市されつつある．

腫瘍組織血管は正常組織血管と異なった性質を有している[26,27]ため，その細胞膜表面若しくは，分泌タンパク質に特異的なタンパク質，いわゆるバイオマーカーが存在している可能性が考えられるが，腫瘍組織血管特異的なバイオマーカー，及びその抗体については世界的に認められる分子はいまだに発見されていないというのが現状である．腫瘍組織血管特異的ではないが，唯一の重要な指標となっているのは血管新生において非常に重要なシグナル系であるVEGFファミリーのVEGFR1（Flt-1），VEGFR2（Flk-1/KDR）の発現上昇のみである．[28-30] そこで本研究では，新規がん治療薬，腫瘍組織血管特異バイオマーカー探索の強力なツールとなり得る，腫瘍組織血管特異タンパク質に対する抗体の創製を従来のハイブリドーマ法と比較して画期的な抗体創製法であるファージディスプレイ法を用いて試みた．

2. ファージディスプレイ法

ファージディスプレイ法は1985年にSmithらによって報告され，[31] バクテリオファージ内に存在するファージミドベクターへ外来遺伝子（ペプチド・タンパク質・抗体等）を導入することで，バクテリオファージ表面に目的分子を発現させることを可能とする技術であり，その分子はバクテリオファージのコートタンパク質（g3p）と融合した形態で発現している．抗体作製への応用は1990年にMcaffertyらが抗体機能ドメインを提示したファージディスプレイ法をハイブリドーマ法に代わる新しいモノクローナル抗体作製技術として報告したことに始まる．[32] 1991年にはMarksらが免疫していないヒトの末梢血リンパ球を出発材料に構築したファージ抗体ライブラリから，ヒト生体成分や，ターキー卵白アルブミン，ウシ血清アルブミンなど異種動物の抗原に対するファージ抗体の分離を報告した．[33]

繊維状ファージM13は環状の一本鎖ゲノムDNAを持ち，そのまわりに5つのコートタンパク質（g3p, g6p, g7p, g8p, g9p）が連結した細長い筒状の構造をしており，大腸菌に感染して増殖するウイルスである．ファージディスプレイは，これらのファージコートタンパクと外来ポリペプチドを融合した形で発現させることでファージ表面にディスプレイさせる方法である．

ファージディスプレイ法の特徴は，① 任意の外来分子をファージ表面に提示できること，② 1個の宿主菌に1個のファージしか感染しないため（pDNA incompatibilityに寄与する），各ファージ内の外来遺伝子とファージ表面に提示された外来遺伝子産物が一致していること，③ 種々の外来遺伝子産物を提示したファージを数億種類以上の多様性を有するライブラリとして容易に，かつ短期間（1週間以内）で調製できること，④ 宿主菌に感染させることで簡便に特定のファージを増幅できることにある．[34,35]

外来遺伝子として一本鎖抗体（single chain variable fragment: scFv）遺伝子を用いるファージ抗体ライブラリは，ファージ表面に数十万から数億以上のレパートリーを有する抗体機能性ドメインであるVL領域とVH領域をリンカーで連結したscFv抗体を発現させるものである（Fig. 1）．このライブラリから標的タンパク質へ特異的に結合するクローンを選択・回収し，増幅する操作（パンニング）を繰り返すことによって，標的タンパク質に結合する

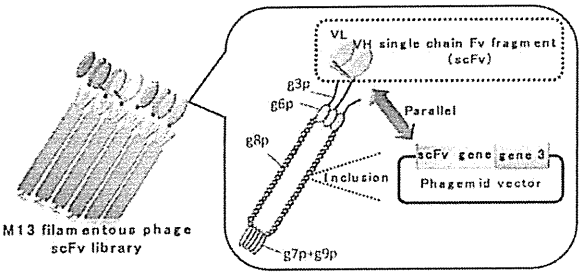

Fig. 1. The scFv Phage Display System

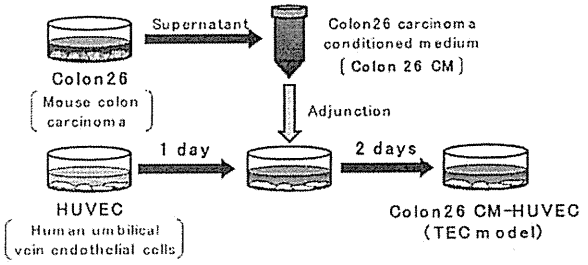

Fig. 2. Development of the Tumor Endothelial Cell Model
Human umbilical vein endothelial cells (HUVEC) cultured in Colon26 carcinoma-conditioned medium (Colon26 CM-HUVEC) were used as model TECs.

scFv 抗体分子を表面提示したファージをスクリーニングすることが可能である.[36,37] しかも得られたファージは目的抗体をコードする遺伝子を内封しているため，抗体の遺伝子配列も同時に獲得することが可能である．このように，ファージディスプレイ抗体ライブラリは *in vitro* で生体内の抗体産生系を模倣し，さらに生体の免疫系から独立した抗原の種類を選ばない優れた抗体創製システムとして，抗体医薬開発に大きく貢献している．

3. 抗腫瘍組織血管抗体の創製

3-1. 腫瘍組織血管内皮細胞モデル　抗腫瘍組織血管抗体を創製するためには，腫瘍組織血管内皮細胞を獲得しなければならないが，腫瘍組織血管内皮細胞のみを生体内腫瘍組織から単離することは非常に困難である．そこで筆者らはがん細胞の培養上清（Conditioned Medium: CM）を用いることで，*in vivo* の腫瘍組織血管内皮細胞を模倣した腫瘍組織血管内皮細胞モデルを *in vitro* の系で再構築し，このモデル細胞から抗原タンパク質を調製後，これを用いて抗体創製を試みた．本検討ではマウス結腸がん細胞（Colon26）の CM で培養したヒト臍帯静脈血管内皮細胞（HUVEC）を腫瘍組織血管内皮細胞モデル（Colon26 CM-HUVEC）とした（Fig. 2）．

この腫瘍組織血管内皮細胞モデルは，生体内腫瘍組織血管内皮細胞に特徴的な性質である細胞間透過性の亢進を示し,[38] また腫瘍組織血管内皮細胞モデルの膜抗原を樹状細胞にパルス後，この樹状細胞をマウスに免疫したところ，*in vivo* において，副作用を引き起こすことなく腫瘍組織血管特異的な傷害性が誘導され，それに伴う抗腫瘍効果が観察された（未発表データ）．さらには，2 次元電気泳動解析により，その特異的抗原タンパク質の存在が明らかとなった（未発表データ）．

これらのことから，この腫瘍組織血管内皮細胞モデルは生体内の腫瘍組織血管内皮細胞と全く同じ特異的抗原タンパク質を発現している可能性が非常に高いと考えられる．

3-2. 腫瘍組織血管内皮細胞モデル免疫抗体ライブラリの作製　現在，ファージ抗体ライブラリとしては，免疫していない動物や健常人の B 細胞を由来とした「ナイーブファージ抗体ライブラリ」[39,40] と免疫した動物や疾患患者の B 細胞を由来とした「免疫ファージ抗体ライブラリ」[41] の 2 種類が主に用いられている．各ライブラリにはそれぞれ長所・短所があり，「ナイーブファージ抗体ライブラリ」は抗体遺伝子に偏りのない多様性に富んだ抗体ライブラリを獲得できるという長所を持つ一方で，抗原結合力の強い抗体を得ることが困難であるという短所も持ち合わせている．また，「免疫ファージ抗体ライブラリ」は抗原結合力の強い抗体を得ることができるという長所を持つ一方で，免疫状態に偏りがあるため，「ナイーブファージ抗体ライブラリ」と比較して得られる抗体ライブラリは多様性に乏しいという短所を持つ．このように両ライブラリは一長一短であるため，目的に合わせて使い分ける必要がある．

本検討では最終的に獲得した抗体を抗原探索・解析のツールとしてだけでなく，ドラッグデリバリーのツールとして用いる狙いがあるため，より強力な結合力を有する抗体を獲得可能な「免疫ファージ抗体ライブラリ」を作製した．

免疫原として腫瘍血管内皮細胞モデルである Colon 26 CM-HUVEC を BALB/c マウスに一週間おきに 2 回免疫を行った．次に，マウスの Colon26 CM-HUVEC に対する抗体価を測定後，脾臓を回収

し，mRNA を回収した．続いて，この mRNA をテンプレートに cDNA を作製し，PCR により抗体の VL, VH 領域の DNA の増幅を行った．さらに，増幅した VL, VH 領域の DNA を連結させる assembly PCR を行い，scFv DNA を作製した．そして，この scFv DNA をファージミドベクター（pCANTAB5E）へクローニングした．最後にクローニング後のファージミドベクターを大腸菌（TG1）へエレクトロポレーションにより導入した．構築したライブラリのライブラリサイズは大腸菌の形質転換効率より算出した．その結果，構築した抗体ライブラリは 1.3×10^7 CFU という抗体多様性を保持していた（Fig. 3）．

3-3. 抗腫瘍組織血管抗体のスクリーニング

機能性分子を獲得するためのスクリーニング系の設計はファージディスプレイ法のみならず，ディスプレイ技術を駆使する場合のキーテクノロジーとして重要視される．精製抗原が入手可能な場合は，固層化法（パンニング）やビオチン化抗原とストレプトアビジン固定化担体を用いたスクリーニング方法が主要な選択系として用いられている．しかし，各スクリーニングを効率よく行うためには，対照抗原の目的エピトープを被覆，あるいは変性させない工夫が必要であり，さらには反応温度や洗浄条件，塩濃度など複数の要因が影響する．

今回，われわれは精製された抗原タンパク質を獲得しているため，抗体ライブラリから抗腫瘍組織血管抗体を選別するスクリーニング系として簡便なパンニングを選択した．パンニングはファージ抗体ライブラリ内から，固層化した標的タンパク質へ特異的に結合するクローンを選択・回収し，増幅する操作であり，このパンニングを繰り返すことによって，標的タンパク質に結合する scFv 抗体分子を表面提示したファージを選別・濃縮することが可能である（Fig. 4）．

近年，臨床で用いられている抗体医薬品は細胞膜表面の膜タンパク質，若しくは血中に遊離している機能性タンパク質（レセプターアゴニスト等）を認識する抗体である．今回創製する抗体の将来的な展望として，創出した抗体をドラッグデリバリー，また診断のツールとして使用することを目的としているため，創製する抗体は細胞内タンパク質ではなく，細胞外表面上の膜タンパク質を認識する抗体であることが必須条件であると考えられる．このことから，われわれはパンニングにより抗体を選別する際に用いる標的抗原には，調製時に破壊された細胞の細胞内タンパク質が混入する恐れのある，細胞抽出抗原タンパク質（細胞ライセート，ブタノール抽出膜抗原タンパク質等）を用いるのではなく，生細胞をそのまま標的抗原として用いることが最適であると考えた．

さらに，抗腫瘍組織血管抗体を創製するにあたって，われわれが非常に重要であると考えていることは，いかに副作用の少ない抗体を選別するかである．腫瘍組織血管は正常組織血管内皮細胞が腫瘍細胞の産出する液性因子（サイトカイン，ケモカイ

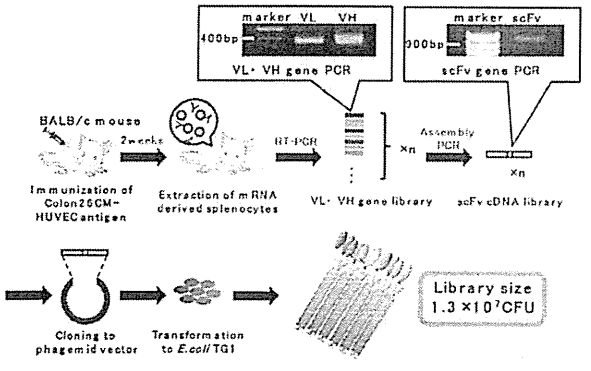

Fig. 3. Development of the Tumor Endothelial Cell Immune Antibody Library

The single chain antibody fragment variable (scFv) phage display library was prepared by amplifying the Fv genes from the mRNA derived from the TEC-immunized murine splenocytes.

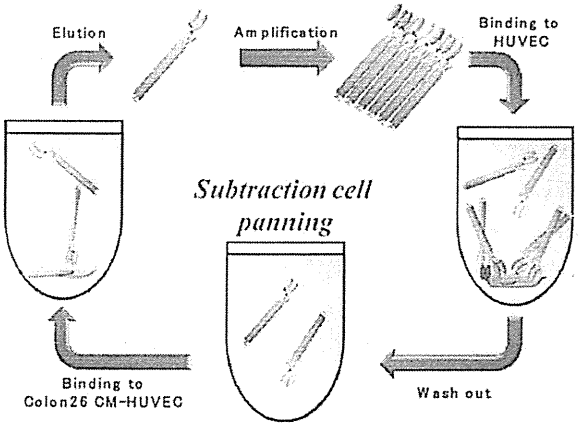

Fig. 4. Antibody Selection by Subtraction Cell Panning

Anti-TEC antibodies were selected by cell panning against Colon26 CM-HUVEC with subtractive panning against normal HUVEC.